LBL--30748

DE92 000655

HEAVY ION FUSION ACCELERATOR RESEARCH (HIFAR)

HALF-YEAR REPORT*

October 1, 1990 - March 31, 1991

Heavy Ion Fusion Staff

Accelerator and Fusion Research

Lawrence Berkeley Laboratory
1 Cyclotron Road
Berkeley, CA 94720

April 1991

* This work was supported by the Director, Office of Energy Research, Office of Basic Energy Sciences, Advanced Energy Projects Division, U.S. Department of Energy under Contract No. DE-AC03-76SF00098.

FOREWORD

The basic objective of the Heavy Ion Fusion Accelerator Research (HIFAR) program is to assess the suitability of heavy ion accelerators as igniters for Inertial Confinement Fusion (ICF). A specific accelerator technology, induction acceleration, is being studied at the Lawrence Berkeley Laboratory and at the Lawrence Livermore National Laboratory.

The HIFAR program addresses the generation of high-power, high-brightness beams of heavy ions, the understanding of the scaling laws in this novel physics regime, and the validation of new accelerator strategies to cut costs. Key elements to be addressed include: 1) Beam quality limits set by transverse and longitudinal beam physics; 2) Development of induction accelerating modules, and multiple-beam hardware, at affordable costs; 3) Acceleration of multiple beams with current amplification without significant dilution of the optical quality of the beams; 4) Final bunching, transport, and accurate focussing on a small target.

TABLE OF CONTENTS

HIGHLIGHTS

R.O. Bangerter

During the last six months the HIFAR Program at Lawrence Berkeley Laboratory has made significant progress. We spent several months on EH&S and associated Tiger Team activities. This effort was very successful. We believe that our buildings and operations are as safe as reasonably possible. The MBE-4 experiments were nearly completed (MBE-4 was shut down in April). We have improved our ability to calculate electric fields produced by complex electrode geometries. We have initiated the development of new types of ion sources. We have also built a 2-meter induction module and have improved our understanding of longitudinal dynamics. Finally, we have made significant progress in improving the ILSE design.

Earlier experiments with MBE-4 demonstrated current amplification up to a factor of about 9. These longitudinal experiments agreed well with our simulations. Errors in the accelerating waveforms caused longitudinal emittance growth; however, the emittance growth when extrapolated to a full-scale fusion driver appears acceptable. Nevertheless, longitudinal control in MBE-4 was more difficult than anticipated. We plan to develop more accurate and more flexible pulsers for future experiments.

Although the study of longitudinal dynamics was the main original goal of MBE-4, the last two years have been primarily devoted to the study of transverse dynamics. In contrast to earlier SBTE experiments that showed no transverse emittance growth, the MBE-4 experiments showed unanticipated emittance growth when the beam was accelerated and bunched. It is important to emphasize that the MBE-4 beams are extremely cold; and allow stringent, sensitive experiments on emittance growth. Specifically the normalized emittance of the MBE-4 beams is $\varepsilon_n \approx 3\pi \times 10^{-8}$ m·rad corresponding to an ion temperature of the order of 0.1 eV. The allowable ion temperature at the end of a driver is of the order of 1 keV. In terms of transverse beam brightness the MBE-4 beams are about 10^3-10^4 times brighter than required at the end of a fusion driver. An extensive theoretical, numerical, and experimental campaign has led to the conclusion that the emittance growth was caused by two factors:

1. Improper matching, centering, and alignment.
2. Transporting beams that are so large that the outer portions of the beam interact with nonlinear dodecapole focusing forces and possibly non-uniform space-charge distributions.

By careful alignment and matching we have now been able to transport accelerated beams without significant emittance growth. Thus, the MBE-4 experiments were concluded on an optimistic note.

The new calculational technqiue for calculating electric fields in complicated 3-D geometries is explained in the contribution by Berz, Fawley and Hahn. The calculations are in good agreement with measurements of effective quadrupole length and dodecapole strength on MBE-4.

The carbon arc sources that have been under development for several years for ILSE are advantageous because they don't require heating. The high temperatures (~1000°C) needed for the MBE-4 alumino-silicate cesium sources would lead to significant thermal, mechanical, and electrical complexity if such sources were used in the ILSE injector. Moreover, we have been unable to obtain adequate beam current of low mass ions such as sodium using these thermionic sources. Unfortunately the carbon arc sources appear to have a limited life of a few tens of thousands of shots. Furthermore, we have been unable to produce an emittance lower than about $2 \times 10^{-6} \pi$ m·rad. We currently believe that the plasma formed by the arc is too noisy to allow substantial reductions in emittance. We have therefore initiated development of r.f. gas sources for ILSE and have continued to improve thermionic sources as a back-up. The gas sources should provide a great deal of flexibility in ion mass. These sources are based on the sources that have already been demonstrated in the MFE Program at LBL.

Although the ILSE Program will test many features of a fusion driver, the ILSE accelerator appears to be too short to provide a meaningful test of possible longitudinal instabilities. We have therefore initiated a major program to build and measure the properties of driver-scale induction modules. The properties of the modules will be used in theoretical and numerical studies of longitudinal dynamics. Initial measurements are given in this report.

About 18 months ago our theoretical studies suggested that there might be hundreds of e-foldings of the longitudinal instability in the accelerator (growth length of the order of 10 meters). It now appears that the theoretical growth lengths can be made as large as several hundred meters by proper choices of linac parameters. We are studying feedback to stabilize the residual instability. Other methods of controlling the instability such as increased momentum spread will be studied in the future. Increased momentum spread will require the development of achromatic focusing systems.

Finally, although results are not presented in this report, we continue to refine the ILSE design. In particular we are developing designs that will allow us to do tests at full-scale line-charge density and beam size. We are also investigating the possibilities of recirculation on ILSE because preliminary studies of recirculating accelerators show a significant cost advantage over conventional linacs; however, a number of key physics issues must still be addressed theoretically before we would be willing to proceed with recirculation experiments on ILSE.

Most of these articles were presented as papers at the Particle Accelerator Conference held May 6-9, 1991 in San Francisco. The exceptions are the note on Survey and Alignment of MBE-4 by Johnson et al. and note by Henestroza and Eylon on the dependency of the beam time-of-flight on the MBE-4 quadrupole voltage.

TIGER TEAM INSPECTION

C. Pike

Our own LBL Self Assessment revealed 422 separate findings in the HIFAR Facilities. By 18 March 1991 all findings were closed except for one Job Order to Laboratory Construction and Maintenance. The Tiger Team did not find anything in the HIFAR Program that we had not already found. Machine Guarding was not included in the total number of findings. The Engineering Division still needs to provide guidance in this area.

As of 29 February 1991 the program had invested $304k in the compliance category and $6k in employee training. The effort from the HIFAR Program was:

Electrical Engineer		3.5 effort month
Electronics Technician		7.6 effort months
Mechanical Designer		2.1 effort months
Mechanical Technician		7.1 effort months
Total effort		20.3 effort months
	or	1.7 effort years

Because of the effort we have a much cleaner and therefore safer working environment and safety awareness has been improved to the point that safety is a way of life. The biggest programmatic impact was felt by the Injector Program. This program was delayed three months by the Tiger effort.

Emittance Variations in Current-Amplifying Ion Induction Linacs*

Thomas J. Fessenden
Lawrence Berkeley Laboratory, University of California, Berkeley, California

I. SUMMARY

Since 1985 the Heavy Ion Fusion Accelerator Research program at the Lawrence Berkeley Laboratory has been studying current amplification and emittance variations in MBE-4, a four-cesium-beam induction linac. This experiment models much of the accelerator physics of the electrostatically focused section of a fusion driver. Four space-charge dominated Cs^+ beams, initially about one meter in length at currents of 5-10 mA, are focused by electrostatic quadrupoles and accelerated in parallel from approximately 200 keV up to one MeV by 24 accelerating gaps. Final currents of 20-40 mA per beam are typical. Recent experiments with extremely low emittance beams (ε_n= 0.03 mm-mRad) have investigated variations of transverse and longitudinal normalized emittance for drifting and accelerating beams. These very strongly tune-depressed beams (σ_0=72°, σ=6°) are difficult to match to the acccelerator so as to avoid emittance growth during acceleration. During transport strong emittance fluctuations are observed in good qualitative agreement with simulations. Warmer beams with less tune depression exhibit little to no emittance growth, show smaller emittance fluctuations, and are much easier to match. A summary of findings from the MBE-4 studies is presented.

II. INTRODUCTION

The Heavy Ion Fusion Accelerator Research Program (HIFAR) at LBL is assessing the multiple-beam induction linac as a inertial fusion driver. In this concept multiple parallel beams of heavy ions are continually amplified in current and in voltage as they are accelerated to the parameters required to ignite an inertial fusion target (≈10 GeV, 500 TW, 10 ns). Control of the lengths of the beam bunches during the acceleration process is one of the key beam dynamics issues of this approach to a fusion driver. The accelerating waveforms must be carefully shaped to shorten the bunch length and to control longitudinal space charge forces while accelerating the beams. Small acceleration errors, particularly troublesome at low beam energies, can lead to current spikes and beam spill and/or to unacceptable increases in beam emittance. A necessary consequence of current-amplifying acceleration is that the focusing system must transport beams whose speed at a focusing element increases by as much as 20% over the time of the pulse.

MBE-4 is a multiple-beam current-amplifying ion induction accelerator. It was built to develop an experimental understanding of this new type of accelerator. Longitudinal beam dynamics in this experiment are similar to those expected in the electrostatic-focused region of a heavy ion driver. Experiments began with the completion of the injector in 1985 and continued for approximately six years through April 1991. Of particular interest were possibilities of interactions between the multiple beams, longitudinal beam control, and the preservation of longitudinal and transverse normalized emittance during acceleration. The main thrust of the first three years of experimentation was longitudinal beam dynamics and control. The last three were mostly concerned with understanding transverse beam control and emittance growth during acceleration. MBE-4 has been very useful in understanding the physics of current-amplifying accelerators and in providing confidence that much larger ion induction linacs can be expected to operate satisfactory. This paper will summarize our findings from MBE-4.

Fig 1 The MBE-4 multiple-beam ion accelerator (CBB 912-1174)

*Work supported by the Office of Energy Research, Office of Basic Energy Sciences, U.S. Department of Energy under Contract DE-AC03-76SF00098.

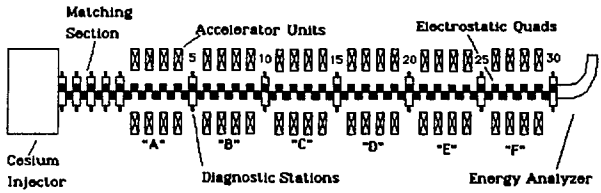

Fig. 2 Schematic of MBE-4.

III. DESCRIPTION

MBE-4 is an induction linac that accelerates four Cs^+ beams from 200 keV at the injector to as much as 875 keV(head); 950 keV(tail) after 24 accelerator gaps with current amplifications as large as nine. Transverse focusing is supplied by four-beam arrays of electrostatic quadrupoles. The initial bunch length is 1.3 m with duration of 2.2 μs. Fabrication of the apparatus was completed in September 1987. A picture of MBE-4 is presented in Fig. 1 and a schematic of the accelerator is given in Fig. 2. The accelerator is 30 periods long. Pumping and diagnostic access are provided at the ends and at each 5th focusing period. Our principal diagnostics are Faraday cups and two-slit scanners which reveal the beam size and emittance for current measurements at each of the diagnostic stations. An electrostatic energy analyzer at the end of the experiment is used to measure the final beam energy and obtain estimates of the longitudinal beam emittance. We also used a small electrostatic energy analyzer that could be inserted at the diagnostic stations to characterize the beam at the input and along the accelerator. During operation the apparatus is pulsed every five seconds. Each pulse is highly repeatable. Every waveform repeats to better than 1 %.

IV. LONGITUDINAL STUDIES AND FINDINGS

Current amplification and longitudinal bunch length control through the accelerator require the use of carefully shaped accelerating voltage waveforms. The method of finding waveforms for accelerating beams in ion induction linacs, was developed by C. Kim [1]. In this current self-replicating scheme, the functional form of the current versus time at a fixed location is preserved through the accelerator and the magnitude increases as the bunch shortens in time. Solutions for the current and the accelerating waveforms at every accelerating gap can be constructed. The charge distribution along the length of the beam bunch generates a longitudinal electric field E_z that will lengthen the bunch if not compensated by the accelerating voltages. The procedure for generating these wave forms including the effects of longitudinal space charge and the finite width of the accelerating gaps were incorporated into a code called SLID which runs on a small computer.

The SLID procedure has proved to be extremely valuable for engineering pulsers for MBE-4 and for understanding and interpreting the results of the experiments. An improved version of the procedure called SLIDE[2] which permits particle overtaking was recently developed by Henestroza. We have found that the SLID and SLIDE calculations of the current and energy waveforms agree very well with experimental measurements [3,4].

To develop the pulsers for controlling and accelerating beams in MBE-4, ideal waveforms from the SLID procedure were first supplied to engineering. As the pulsers were fabricated, the outputs of the pulsers were measured and used as input to the SLID code to generate downstream waveform requests that tended to compensate for unavoidable upstream synthesis errors. Our method of synthesizing waveforms was to add the outputs of several pulsers so as to generate the waveform asked for by the SLID procedure as well as possible. An example of this synthesis is presented in figure 3. Here the outputs of four pulsers are added at gap 11 to generate the waveform requested by the SLID procedure. As can be seen, small errors are inevitably generated as each pulser is energized. Waveforms to provide control of the bunch ends are not present at each accelerating gap but rather are provided at every five to seven gaps.

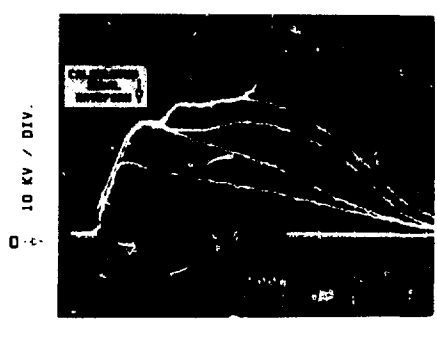

Fig. 3. Synthesis of MBE-4 accelerator wave forms. The outputs of four pulsers are added to produce an accelerating voltage close to that requested by the SLID acceleration procedure

Amplifying current waveforms obtained in MBE-4 are shown in Fig. 4. Here the current of each of the four beams increases from 10 mA at 0.2 MV at the accelerator input to over 90 mA at end of the accelerator. At exit the beam energy increases approximately linearly from 650 kV at the head to 750 kV at the tail. The effect of the acceleration errors can be seen in these waveforms.

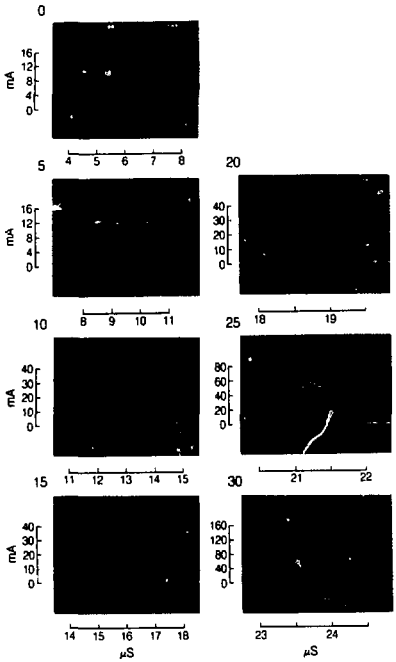

Fig 4. Current amplification from 10 to 90 mA/beam in MBE-4. Each oscillogram shows several pulses.

A better understanding of the effects of errors can be obtained by considering space charge waves on a heavy ion beam. According to Warwick[5] et al., space charge waves in the long-thin geometry of a heavy ion accelerator propagate without dispersion at a speed v_p in the beam frame of

$$v_p = g^{1/2}(\omega_p a/2) \qquad (1)$$

where ω_p is the beam-plasma frequency, a is the beam radius and g is a factor ($\approx$2) that depends weakly on geometry. For MBE-4 the space charge wave speed is a few percent of the beam speed which, relatively, is only three to ten times faster than in a driver. An acceleration error δV generates a space charge wave that separates into forward and backward traveling waves in the beam frame. These produce a current modulation if the waves are allowed to split as the beam travels through the accelerator. This current modulation[6] is given by

$$\delta I = \frac{I}{V}\frac{(v_0^2-v_p^2)}{4v_0v_p}[\delta V(z-v_pt) - \delta V(z+v_pt)] \qquad (2)$$

where v_0 is the beam speed, V is the kinetic beam voltage and I is the beam current. Corrections must be applied before the waves split and the error turns into a current modulation. This will occur in a distance L along the accelerator given approximately by

$$L \approx \frac{1}{4}\frac{v_0^2}{v_p}\Delta t \qquad (3)$$

where Δt is the duration of the error which is assumed short compared with the pulse width. These phenomena are most troublesome at the front of an accelerator where the beam wave speed are lowest. For errors about one microsecond in duration this distance is 2.8 m in MBE-4 and 6 m toward the low end of a driver.

The energy analyzer at the end of MBE-4 is used to measure the beam energy versus time and to estimate the longitudinal emittance growth that has occurred during acceleration. The energy resolution of this instrument is better than 0.5 %. Because the current is amplifying, the beam energy at the end of MBE-4 increases from 650 kV at the head to 750 kV at the tail for the acceleration data presented in Fig. 4. The area of the ellipse that encloses this curve is approximately $4\pi \times 10^{-3}$(Vsec). These measurements when extrapolated to the final focus in a driver[7] yield an expected momentum spread of $\Delta p/p \approx 1.5 \times 10^{-3}$ -- well within the 1% permitted by target focusing considerations. This rather long extrapolation assumes that subsequent acceleration errors are not correlated and are similar in magnitude to those experienced in MBE-4.

V. TRANSVERSE STUDIES AND FINDINGS

Since approximately August of 1988, the preservation of normalized emittance with acceleration has been the principal issue studied with MBE-4. We had observed during the longitudinal experiments that the transverse emittance remained approximately constant or increased with drift or acceleration implying that the normalized emittance was increasing. Moreover, although each emittance measurement could be repeated to within about 5% if done immediately, measurements over long periods varied by factors of 1.5 to 2.

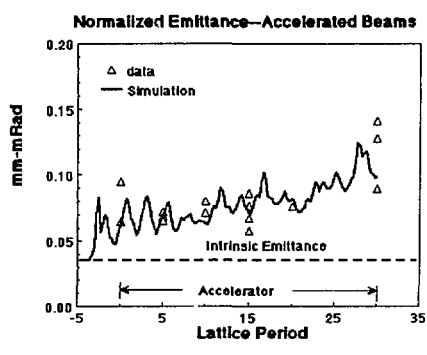

Fig. 5 Measurements and simulation of normalized emittance along MBE-4. The intrinsic emittance is that determined by the source temperature ($\approx$ 1000°C) and beam radius.

Figure 5 shows data collected from accelerated beams at an initial current of 10 mA per beam over a period of several months. Very similar emittance variations obtained from 2-D PIC simulations of strongly tune-depressed beams drifting in electric-quadrupole-focused transport systems had been reported previously by Celata[8]. These simulation studies were continued and extended to accelerating beams by K. Hahn. We define normalized emittance as $\varepsilon_n = 4\,\beta\gamma\,\varepsilon_{rms}$ where ε_{rms} is given by

$$\varepsilon_{rms} = \left[\langle x^2\rangle\langle x'^2\rangle - \langle xx'\rangle^2\right]^{1/2} \qquad (4)$$

A simulation in which the measured beam in phase space at the output of the injector was used to load the code is also presented in Fig. 5. The intrinsic beam emittance as determined by the source radius r_s and the rms thermal velocity v_ϕ at a temperature of 0.1 eV was used at the start of the simulation. The initial emittance growth is due to a space-charge-driven re-arrangement of particles in the beam[9]. Diagnostic access and, consequently, emittance measurements are limited to every 5th lattice period. Because of the sparse sampling and the rapid fluctuations in emittance, the measured emittance can both increase and decrease along the accelerator.

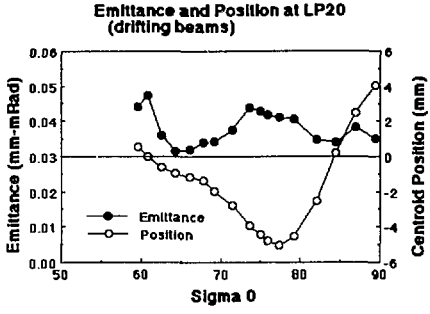

Fig. 6. Variations of beam position and emittance versus focusing strength at lattice point 20. By varying focus strength the beam fluctuations are brought to the point of diagnostic access.

To demonstrate that the rms emittance was rapidly varying along MBE-4, measurements of beam offset and emittance versus the strength of the focusing lattice (σ_0) at fixed position were performed. This technique (which was suggested by D. Keefe) showed that the beam was oscillating back and forth in the channel with an amplitude of 4 to 5 millimeters or nearly 20% of the channel aperture as shown in Fig. 6. This experiment also confirmed that the rms beam emittance was strongly modulated at what corresponds to 2.3 lattice periods in excellent qualitative agreement with the simulations.

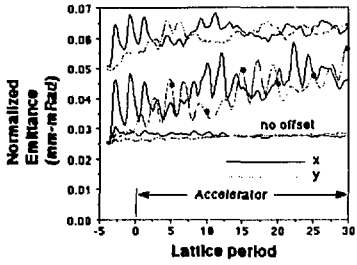

Fig. 7 Beam emittance variations in the x and y planes for offset beams drifted through MBE-4 obtained from code simulations.

Figure 7 shows the x and y normalized emittance versus z obtained from simulations of strongly tune-depressed beams in MBE-4. Except for the case of no offset, the beams were started 3 mm off axis, slightly more than 10% of the channel aperture, with equal x and y deflections. For the lower curves the simulations were started at the intrinsic beam emittance. The dots on the y emittance plot signify the emittance that might be measured at the points of diagnostic access. A simulation at twice the intrinsic emittance which is close to the final emittance of the first off-axis case is also given. These simulations suggest that strongly tune-depressed beams conserve normalized emittance if held to the system axis. Off-axis low-emittance beams exhibit large modulations in rms emittance and a net growth in passing through the transport system. At increased initial emittance, the modulations are less severe and the growth less significant. This behavior was experimentally checked[10] by approximately doubling the beam emittance at injection with a biased grid pair and measuring emittance growth through MBE-4. Reduced emittance growth was recorded as predicted by the simulation.

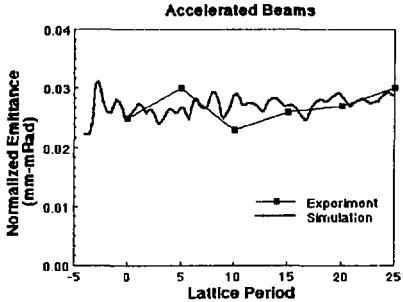

Fig. 8 Measurements and simulation of normalized emittance during acceleration through MBE-4. For these experiments the beams were very carefully matched, centered and aligned in the focusing channel.

Recent MBE-4 experiments have concentrated on carefully matching and centering the beams in the channel to demonstrate current amplification at constant normalized emittance. A second steering array was placed at the entrance to the accelerator that, with the first array at the injector output, centered and aligned the beam on axis. In our initial attempt[11], the beam was centered but not adequately matched. As a consequence, emittance growth was observed. Only after carefully matching, centering, and aligning the beams could these very cold beams be accelerated at constant normalized emittance. Figure 8 shows measurements of normalized beam emittance versus position and a comparison with simulation. Much more information on these experiments is presented in the paper[12] at this conference by T. Garvey et al.

VI. DISCUSSION

The MBE-4 experiments were performed to obtain practical experience with a current amplifying multiple-beam ion induction linac. One of the initial concerns was possible interactions between the beams as they were accelerated or transported through the accelerator. With the exception of a weak interaction in the injector where the beams are at low energy and "see" each other for some distance, no such effect was observed. At low energy the beams interact primarily through their radial space-charge electric fields. These are easily controlled by radial shorting planes along the accelerator which are present for other reasons. At high beam energy, magnetic interactions play a stronger role and some periodic beam coupling phenomena could conceivably arise. The major multiple-beam issue encountered in these experiments was the diagnostic complexity associated with working with many beams.

Current amplification in an induction linac is possible and the beams can be controlled longitudinally with the accelerating waveforms. However, longitudinal control in MBE-4 was more difficult than we anticipated. The accelerator pulsers used for MBE-4 are based on conventional thyratron-switched pulse forming lines. This type of pulser does not have adequate waveform flexibility to easily control the beams longitudinally. Future ion induction linacs will require more agile correction or compensating pulsers every few accelerating gaps--particularly at the low energy end.

Beam space charge greatly reduces the impact of longitudinal acceleration errors as can be seen from Eq. 3. At very low beam intensities the response to an error becomes large with time or drift length. The acceleration errors can be repaired or compensated downstream if corrections are made before the forward and backward space charge waves on the beams can split. Although these corrections contribute to the longitudinal temperature of the beams, the scaling formulas suggest that these will not unduly compromise the final focusing of the beam onto the target.

Transversely, very cold space-charge dominated ion beams can be accelerated at constant normalized emittance at least over the length of MBE-4 if great care is taken to match, center, and align these beams in the transport channel. However, for long linacs or drivers, extreme care may not be required. These experiments and simulations suggest that for sufficiently long system, the beams will center and match themselves with an accompanying increase in emittance. This emittance growth may be affordable. Further study is required (experiments, theory, simulation) to determine if this so.

VII. ACKNOWLEDGEMENT

The work presented here is a summary of the efforts of much of the LBL HIFAR group since 1985. Notable among these are A. Warwick, and C. Kim who made major contributions to the design of MBE-4 and to the longitudinal studies; H. Meuth, S. Eylon, and T. Garvey who concentrated more on the transverse studies; K. Hahn, E. Henestroza, L. Smith, A. Faltens and more recently W. Fawley who provided the theoretical guidance and simulation backup; and last but far from least was D. Keefe who contributed in every conceivable way to the MBE-4 experimental program.

VIII. REFERENCES

[1] C.H. Kim and L. Smith, "A Design Procedure for Acceleration and Bunching in an Ion Induction Linac" Part. Accel. 85, pp 101-113.

[2] E. Henestroza, "Study of the Longitudinal Ion Dynamics Extended Version; SLIDE"HIFAR Year End Report 1989

[3] T.J. Fessenden, D. Keefe, C. Kim, H. Meuth, and A. Warwick, "The LBL Multiple Beam Experiments" IEEE PAC Cat. No. 87CH2387-9, Vol. 2, pp. 954-956

[4] A.I. Warwick, D.E. Gough, D. Keefe, and H. Meuth,"Acceleration, Current Amplification and Emittance in MBE-4, an Experimental Beam Induction Linear Accelerator for Heavy Ions," Proc. 1988 Linear Accelerator Conf., p. 51, Oct. 88.

[5] A.I. Warwick, T.J. Fessenden, D. Keefe, C.H. Kim, H. Meuth, "Performance of MBE-4, an Experimental Multiple Beam Induction Linear Accelerator for Heavy Ions,", Proc. European Particle Accelerator Conference, p. 118, June 1988.

[6] E.P. Lee, private communication.

[7] A.I. Warwick, D.E. Gough, and H. Meuth, "Preliminary Report on MBE-4, an Experimental Multiple-Beam Induction Linear Accelerator of Heavy Ions." LBL Report 28529, November 1988.

[8] C.M. Celata, "The Effect of Nonlinear Forces on Coherently Oscillating Space-Charge-Dominated Beams" IEEE PAC Cat. No. 87CH2387-9, Vol. 2, pp. 996-1000.

[9] T.P. Wangler, K.R. Crandall, R.S. Mills, and M. Reiser, "Relation between Field Energy and RMS Emittance in Intense Particle Beams," IEEE Trans. on Nucl. Science, NS-32, (1985)

[10] S. Eylon, E.R. Colby, T.J. Fessenden, T. Garvey, K. Hahn and E. Henestroza, "Emittance Variations of Very Cold Ion Beams During Transport Through MBE-4," to be published in Part. Accel.

[11] T. Garvey, S. Eylon, T.J. Fessenden and E. Henestroza, "Beam Acceleration Experiments on a Heavy Ion Linear Induction Accelerator (MBE-4)," to be published in Part. Accel.

[12] T. Garvey, S. Eylon, T.J. Fessenden, K. Hahn, and E. Henestroza,"Transverse Emittance Studies of an Induction Accelerator of Heavy Ions," these proceedings

Transverse Emittance Studies of an Induction Accelerator of Heavy Ions

T. Garvey, S. Eylon, T.J. Fessenden, K. Hahn, and E. Henestroza

Lawrence Berkeley Laboratory,
Berkeley, California 94720

ABSTRACT

Current amplification of heavy ion beams is an integral feature of the induction linac approach to heavy ion fusion. As part of the Heavy Ion Fusion Accelerator Research program at LBL we have been studying the evolution of the transverse emittance of ion beams while they are undergoing current amplification, achieved by longitudinal bunch compression and acceleration. Experiments are conducted on MBE-4, a four beam Cs^+ induction linac. The space-charge dominated beams of MBE-4 are focused by electrostatic quadrupoles while they are accelerated from nominally 200 keV up to ~ 1 MeV by 24 accelerating gaps. Initially the beams have currents of typically 4 mA to 10 mA per beam. Early experimental results showed a growth of the normalized emittance by a factor of 2 while the beam current was amplified by up to 9 times its initial value. We will discuss the results of recent experiments in which a mild bunch length compression rate, more typical of that required by a fusion driver, has shown that the normalized emittance can be maintained at its injection value (0.03 mm-mr) during acceleration.

1. INTRODUCTION

The induction linac approach to heavy ion driven inertial fusion envisages a design in which multiple beams are employed at the low energy end of the driver with the beam current undergoing amplification as it is accelerated. Current amplification results both from the increase in particle velocity and also from longitudinal bunch compression. This compression is achieved by applying a velocity 'tilt' between the head and tail of the bunch, provided by tailored voltage waveforms applied at the accelerating gaps. MBE-4 is a four beam Cs^+ linac built to investigate longitudinal dynamics issues related to this concept. The linac is comprised of a 30 period, electrostatic, AG focusing lattice. Each doublet is followed by an accelerating gap with the exception of every fifth doublet where the gap is reserved for diagnostic access and vacuum pumping. Each lattice period (l.p.) is 45.7 cm long resulting in a linac of 13.7 metres.

Early experiments on MBE-4 concentrated on a demonstration of current amplification while maintaining control of the current profile and correcting for inevitable acceleration 'errors', which arose from the difference between ideal accelerating pulser waveforms and those waveforms achieved in practice. These experiments, in which the current was amplified from 4x10 mA to 4x90 mA and the energy increased from 200 keV (the injection value) to 900 keV, were accompanied by a growth in the normalised emittance by a factor of approximately two. This work has been reported previously and a review can be found elsewhere in these proceedings[1].

2. EXPERIMENTS

We have identified a number of mechanisms which may be responsible for emittance growth in MBE-4 including matching errors, rapid longitudinal compression (leading to a change in the space-charge electrostatic-field energy), and non-linear field effects (self-fields, image-fields, focus fields). The last of these mechanisms is particularly troublesome for off-axis beams where the edge of the beam may approach the non-linear field region of the quadrupoles[2]. For the experiments discussed here offsets are minimised by the use of steering elements at the entrance to the linac and by careful alignment of the accelerator. Proper matching of the beam phase-space to the lattice of the linac is performed by adjustment of a "matching section" consisting of eight electrostatic quadrupoles just downstream of the diode.

Recent experiments have involved the application of an acceleration schedule which results in a smaller increase in the beam line charge density between injection and full energy. In order to realise this we have reduced the extent of the applied velocity tilt in the early gaps of MBE-4 with the majority of the acceleration being provided by waveforms in which the voltage does not vary greatly during the passage of the beam pulse. bunch compression in these experiments means that the beam pulse length is not sufficiently short for the final accelerating waveforms to completely straddle the beam pulse. Consequently the current waveforms observed in these experiments are poorer than those obtained in earlier studies, however as we are concerned here with transverse dynamics this is not a serious concern.

In attempting to maintain a matched beam during acceleration we scale the strengths of the quadrupole focusing voltages, V_q, such as to keep them proportional to the beam line-charge density, λ, i.e. $V_q \sim \lambda \sim I / v$, where I and v are the beam current and velocity respectively. The beam currents and velocities used in calculating the required quadrupole voltages are determined approximately for any given acceleration schedule using a longitudinal dynamics simulation

Work supported by the Office of Energy Research, Office of Basic Energy Sciences, U.S. Department of Energy. Contract DE-AC03-76SF00098.

code (SLID) which uses the measured beam current and energy at injection as input. The available range of quadrupole voltages is limited by breakdown and such scaling would not have been possible in the early experiments where λ was increased by a factor of ~ 4.5

Diagnostics and Data Reduction

Transverse emittance measurements are made using the familiar double slit technique with a multi-shot scanning procedure to determine the signal strength as a function of the transverse (x,x') phase space position, the charge being collected in a Faraday cup behind the downstream slit. Measurements can be made in each transverse plane in turn with typically 400 shots required to obtain one value of emittance. The charge collected through both slits is recorded many times (20 to 50) during the pulse so as to provide a time resolved measurement of the emittance. The data collected can be reduced to yield other time resolved quantities of interest such as the beam size, centroid motion and current profile integrated along the direction of the slits. A typical set of data for the beam at injection is shown in Fig.1. The four traces show the beam current (top left), beam emittance (top right), r.ms. beam size (bottom left, upper), centroid position (bottom left, lower), the r.m.s. slope of the beam (bottom right, upper) and the angular off-set of the centroid (bottom right, lower).

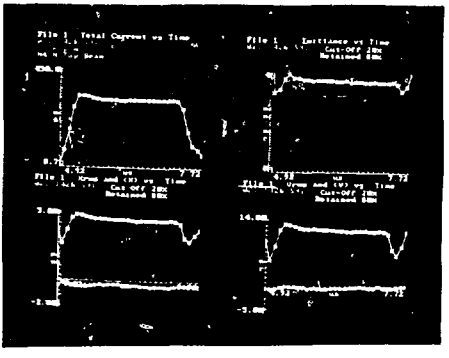

Figure 1. Time-resolved measurements of MBE-4 beam parameters. See text for expianation of traces.

Figure 2 shows a typical emittance plot at the entrance to the linac for a fixed time within the beam pulse.

In calculating the emittance we define the r.m.s. value ε_{rms} as,

$$\varepsilon_{rms}^2 = \langle (x - \langle x \rangle)^2 \rangle \langle (x' - \langle x' \rangle)^2 \rangle - \langle (x - \langle x \rangle)(x' - \langle x' \rangle) \rangle^2 , \quad (1)$$

with the normalised emittance, ε_n, being defined as,

$$\pi\varepsilon_n = 4\pi\beta\varepsilon_{rms}. \quad (2)$$

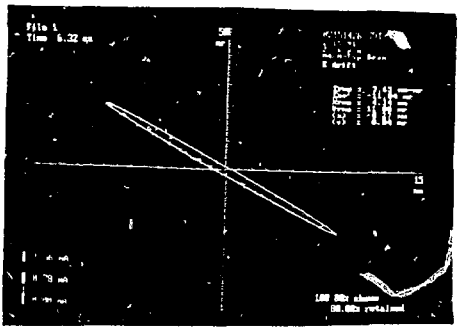

Figure 2. Phase space data at injection to the linac. The ellipse corresponds to a K-V beam of the same emittance as the measured beam.

During operation of the acceleration pulsers the signals obtained on the Faraday cups contain contributions from electrical noise which can be dominant at the edge of the phase space plots where the signal due to the beam is low. In order to exclude such effects we refer to the emittance contained in a given percentage, P, of the beam current where,

$$P = \Sigma_{i,j} S(x_i,x'_j,t)\ U(S(x_i,x'_j,t) - c) \,/\, \Sigma_{i,j} S(x_i,x'_j,t) , \quad (3)$$

In equation (3) U is a unit-step function and the constant c is is a cut-off signal level determined by iteration to correspond to the desired P. The averages used in equation (1) are calculated using only signals above the cut-off value. Typically we find that 80% values are useful for quoting the emittances of accelerated beams while 90% is usable for drift beams. Figure 3 shows a plot of the calculated emittance as a function of P where it is quite apparent that the computed value increases non-linearly with P above P = 80%.

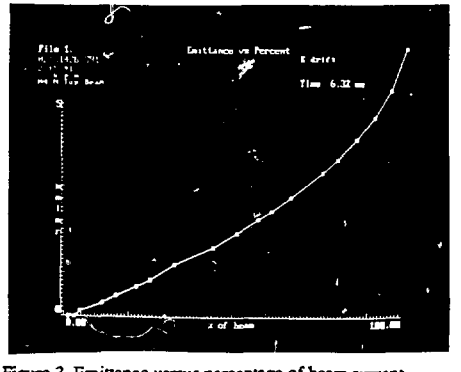

Figure 3. Emittance versus percentage of beam current.

3. RESULTS

Following the installation of a current limiting aperture we have been working with smaller beam currents (< 5 mA) which, at injection, typically have ϵ_n = 0.03 mm-mrad (P = 90%) [3]. The aperture was employed to remove beam particles which were over-focused due to aberrations in the diode optics. The resulting beam radius is nominally 10 mm, propagating in a transport channel of 27 mm radius. For our 'mild' acceleration schedule the measured currents and computed energies at the diagnostic stations are given in Table 1. The corresponding emittances measured under both drift and acceleration in the horizontal plane are shown in Fig. 4 for P = 80%. One can see that, within the limits of experimental error, the normalised emittance is conserved. For this schedule the energy is increased by a factor of 2.6 while λ is increased by only 18%. The 'missing' point for the acceleration data at l.p. 30 is due to faulty and irreproducible behaviour of the principal accelerating pulser in the last section of the machine.

Table 1.
Energy and current vs. l.p.

l.p.	Current (mA)	Energy (keV)
0	3.7	186
5	4.0	190
10	4.2	245
15	5.1	270
20	6.2	390
25	7.0	480

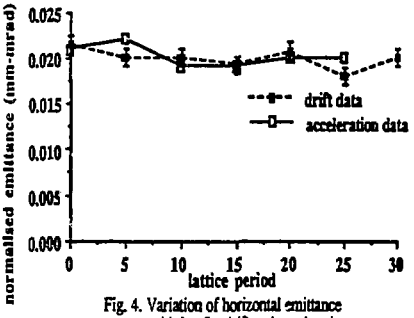

Fig. 4. Variation of horizontal emittance with l.p. for drift and acceleration.

4. DISCUSSION

We have previously reported emittance growth for our 3.7 mA beam under a stronger compression (x 3) but that data was complicated by poor matching from the injector (the matching section having been adjusted for the more usual current of 5 mA)[4]. For the data discussed in this paper the drift beam has been properly matched to the linac, however, it is apparent from measurements of the beam envelope under acceleration that the beam is becoming mismatched in the latter part of the machine. More careful matching under acceleration might require the use of accurately measured currents and energies, as opposed to the SLID calculated values, to determine the quadrupole voltages. An up-graded version of SLID (SLIDE) has been developed which gives improved agreement with the measured data and which might be used for better matching in future experiments on heavy ion induction linacs. Proper matching at injection is found to be neccessary however to minimise emittance growth for both drift and accelerated beams over the length of the linac.

Despite the mismatch under acceleration we find that, for well centered beams with sufficiently mild compression, the normalised emittance can be kept constant during acceleration. Our experiments, however, have not led us to an allowable limit for the rate of compression. Recently we have obtained data which shows that the line density can be doubled while the energy is increased by the same factor as above without much growth in the emittance. This is in contrast to early experimental data from MBE-4 where emittance growth of 75% was seen in another acceleration schedule which doubled the line density. The greater attention paid here to maintaining a well centered beam may be the beneficial factor in the new data. The maximum beam offset observed in our experiments is approximately 1.5 mm which is consistent with residual injection offsets and the limits of the alignment of the focus elements (±0.13 mm). The observed variations in emittance growth under different conditions of mis-match, beam offset and current amplification are found to be in reasonable agreement with the results of 2-D particle-in-cell simulations[1]. Thus we are confident that our computer code can accurately predict the expected growth of emittance in future induction linac designs.

5. ACKNOWLEDGEMENTS

We are indebted to L. Smith, A. Faltens and W.M. Fawley for helpful discussions.

6. REFERENCES

[1] T.J. Fessenden, "Emittance variations in current-amplifying induction linacs", invited paper in these proceedings.
[2] T. Garvey et al., "Transverse beam dynamics studies of a heavy ion induction linac", Proceedings of the 1990 Linac Conference, Albuquerque NM, September 1990, pp 752-754.
[3] T. Garvey et al., "Multiple beam induction linac studies at LBL", Proceedings of the High Power Beams Conference, Novosibirsk, July 1990, pp 1277-1282.
[4] T. Garvey et al., "Beam acceleration experiments on a heavy ion linear induction accelerator", to be published in Particle Accelerators.

Drift Compression Experiments on MBE-4 and Related Emittance Growth Phenomena*

S. Eylon, A. Faltens, W. Fawley, T. Garvey, K. Hahn, E. Henestroza, and L. Smith,
Lawrence Berkeley Laboratory, 47/112
University of California
Berkeley, CA 94720 USA

Abstract

We have recently conducted a series of experiments on the MBE-4 heavy ion accelerator in which a velocity tilt was placed on the beam in the first accelerating section beyond the injector, followed by drift compression over the remaining 11 meters. Depending upon the magnitude of the velocity tilt and the accompanying mismatch in the focusing lattice, emittance growth was observed, manifested by "butterfly" shapes in $x - x'$ phase space. We discuss various analytical limits on ion beam compression and relate them to these experiments and also to a driver for a heavy ion fusion reactor. We also present numerical simulations which investigate various aspects of compression and consequent emittance growth.

I. Introduction

MBE-4 is a multiple beam, heavy ion accelerator at LBL designed to study the physics of space-charge dominated beams and scaling thereof to a heavy ion fusion "driver". One of the major requirements for a driver is smooth and controlled compression of the heavy ion beam from a typical duration at the injector ($E \sim 2-10$ MeV) of $\sim 10\mu$sec to a duration at accelerator exit ($E \sim 5-10$ GeV) of $\sim$ 100ns. In general, this temporal compression will involve a smaller, but not insignificant increase in line charge density also. There is an additional $\sim$ 10x compression at nearly constant energy between the accelerator and target to bring the pulse duration to the wanted 10 ns.

In the last year, we have conducted a number of compression experiments on MBE-4 both at constant energy (*i.e.* drift compression) and with steady acceleration [1] from the injector energy of 185 kV to final energies of $\sim$ 800 kV. In both cases, the compression is achieved via a head-to-tail velocity tilt on the beam. Of particular concern is the behavior of the ion beam transverse phase space during the longitudinal compression. Our results suggest that very strong compression ratios ($\geq 6:1$) lead to substantial emittance growth for MBE-4 beams while smaller ratios ($\leq 3:1$) generally cause little or no emittance growth. As explained in §IV, the key physics appears to be the interaction between a highly compressed and thus radially large beam and the external nonlinear dodecapole focusing forces and internal, nonlinear space charge fields.

*Work supported by the Director, Office of Energy Research, Office of Basic Energy Sciences, Advanced Energy Projects Division, U.S. Dept. of Energy under Contract No. DE-AC03-76SF00098.

II. Experimental Set-up

For the drift compression experiments described here, MBE-4 was used in a single beam mode with the 185-kV injector producing a 2.5-μs duration, 8-mA current pulse of Cs^{+1}. As the beam leaves the injector, it passes through a "matching zone" composed of a eight individual quadrupoles used for transition onto the syncopated FODo focusing lattice of the main accelerator. Within this matching zone, there is an aperture plate that absorbs the outer (and most badly aberrated) portions of the beam, reducing the current by a factor of two. In general, the matching is imperfect and the beam's radial profile shows low level hollowing oscillations between lattice period 0 (≡LP0) and LP10. The electrostatic quadrupole voltages were set to produce a single particle phase advance σ_0 of 72° per lattice period; the space-charge depressed tune σ was in the range $7 - 10°$.

The first four accelerating gaps were timed so that a nearly linear velocity tilt (ranging from 0 to $\geq$ 12%) was put on the beam. We used a numerical code SLIDE[1] to determine the timing and amplitude of the accelerating pulses. No further acceleration fields were applied downstream and thus the beam energy remained constant apart from the work done against the longitudinal space charge field. An energy analyzer (normally positioned at LP5) measured the temporal variation of the beam's energy with a 0.5% energy and $\leq$20-ns temporal resolution. At every five lattice points along the accelerator, a two-slit emittance scanner determined the $x - x'$ projection of the beam's transverse phase space. In general, the x resolution of $\approx$ 1.0 mm was much smaller than the typical beam radius of 5-10 mm, while the angular resolution of 0.7 mrad was comparable to the projected RMS width. The emittance scans were programmed to trace out a parallelogram in phase space with a tilt equal to that corresponding to the temporal center of the beam's phase space ellipsoid.

III. Results

Our initial drift compression experiments were with a quite vigorous acceleration schedule which resulted in a nearly 5:1 current increase by LP15, and 7.4:1 by LP20. The RMS emittance also tripled and butterfly shapes were evident in the phase space data. We then ran a number of less vigorous compression schedules to determine the sensitivity and behavior of the emittance increase.

Table 1. Emittance (ε) and beam radius (a) measurements for drift compression experiments

I_{max}/I_0	$\varepsilon^{rms}_{max}/\varepsilon^{rms}_0$	a_{max}/a_0	$\varepsilon^{\mu}_{max}/\varepsilon^{\mu}_0$	N_{max}
1:1	0.9-1.1	1.0-1.2	1.1-1.2	–
1.5:1	0.9-1.1	0.9-1.0	1.0	≥LP20
3.7:1	1.3-1.6	1.6	1.0-1.2	LP25
7.4:1	≥2.8-3.2	≥1.7-2.0	≥2.1	LP20

Table 1 presents various measured quantities summarizing the results of the different compression schedules. The "microscopic" emittance ε^{μ} is defined to be the phase space area (not necessarily contiguous) occupied by the most intense 80% fraction of the beam current. This quantity is readily extracted from the 2D map produced by the emittance scanner. ε^{μ} is expected to be a more "conserved" quantity than ε^{rms} in cases such as a simple "S" distortion of the $x - x'$ phase space. N_{max} is the lattice period at which maximum compression was measured. For the 7.4:1 compression data, it appears that portions of the beam extended outside the maximum range scanned in x, ±20 mm (the clear quadrupole aperture is 27.4 mm).

In Fig. 1 we plot $\varepsilon(z)$ for various longitudinal slices of the beam pulse in the 3.7:1 compression experiment. The slices are labeled by their charge-weighted positions in the beam with the presumption that no longitudinal overtaking has occurred. Two observations are of note: 1. Slices with little compression ($I/I_0 \leq 2.7$) suffered little emittance growth and those in free expansion near the head and tail may actually have "cooled off" with increasing z. 2. The mid-pulse slices with significant emittance growth by LP25 showed little growth at earlier positions in z where the compression was ≤ 3.0.

This first observation is also true for the 7.4:1 compression data although the sparsity of observation points (LP0-LP20 only) prevents one from drawing firm conclusions concerning the final state of the beam. Moreover, both high compression cases show that the "microscopic" transverse phase space areas of the beam increased far less than did the RMS measures. For the 3.7:1 case, the relative increase in ε^{μ} is essentially unchanged from that measured for the simple 1:1 drift case. Figure 2, which plots phase space contours of a central beam slice at LP25, shows why this is so: the phase space ellipse has developed "S"-arms which account for the increase in RMS emittance but do not result in an actual phase space dilution. By contrast, Fig. 3, which plots phase space contours for the central slice of the 7.4:1 compression case, shows a "butterfly" or bow tie shape in its wings. The butterfly wings include both a major portion ($\geq$ 30%) of the current at a given instant in time, and persist for the great majority of longitudinal slices measured at LP20. In this case, $x - x'$ phase space has been truly diluted and no simple system of lenses will reverse this degradation.

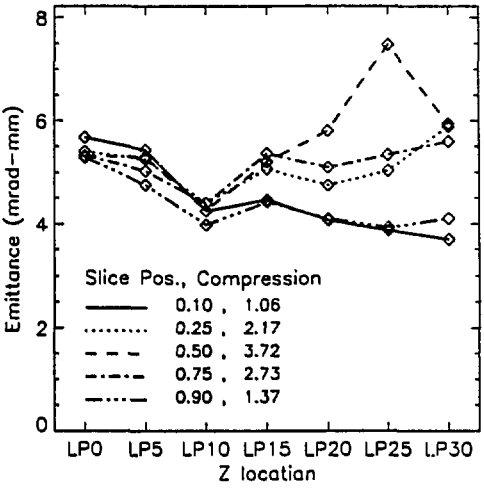

Figure 1: RMS emittance measurements for various longitudinal slices in the 3.7:1 drift compression data. The first number refers to the charge-weighted position in the beam (*i.e.* head=0, mid-pulse=0.5, tail=1) while the second refers to the maximum compression measured for a given longitudinal slice.

IV. Analysis and Discussion

After discovering the butterfly shapes in the high compression phase space data, some of us suspected that longitudinal overtaking might be occurring within the beam near the LP15-LP20 region. Supporting this view was an observed rapid temporal change in the phase space ellipsoid tilts, exceeding 90° in a time half that of the current pulse FWHM. Perhaps the butterfly shapes were actually the superposition of two beamlets of different energies whose integrated phase advance differed by ~ 90°. However, the **SLIDE** numerical code, which has been quite successful in predicting current waveforms for MBE-4 compressed beams, did not suggest problems with overtaking. Furthermore, energy analyzer scans taken at LP15 and LP20 do not show obvious double-valued behavior that would be a sign of longitudinal overtaking.

A related possibility is that while no longitudinal overtaking *per se* occurred, the longitudinal beam compression might have become so great in the 7.4:1 case that the *longitudinal* variation in the z-integrated phase advance for mismatch oscillations has become significant ($\geq$ 1 radian) over a quadrupole aperture radius b. If so, this allows "communication" via space charge fields between slices of different mismatch phase and might lead to relatively rapid phase mixing. For our case of $\sigma \ll \sigma_0$, we estimate the

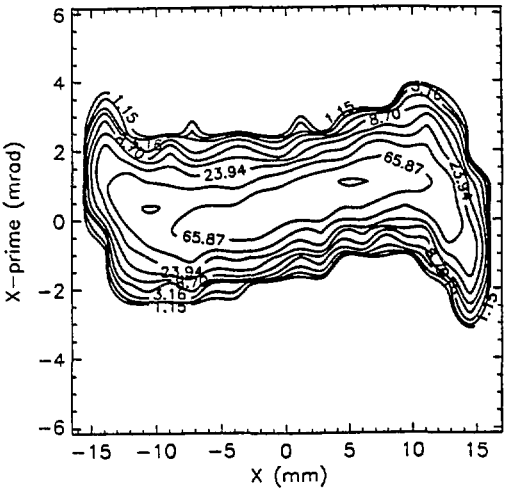

Figure 2: Phase space density contours (equi-spaced logarithmically) measured at LP25 for the central longitudinal slice of the 3.7:1 drift compression data.

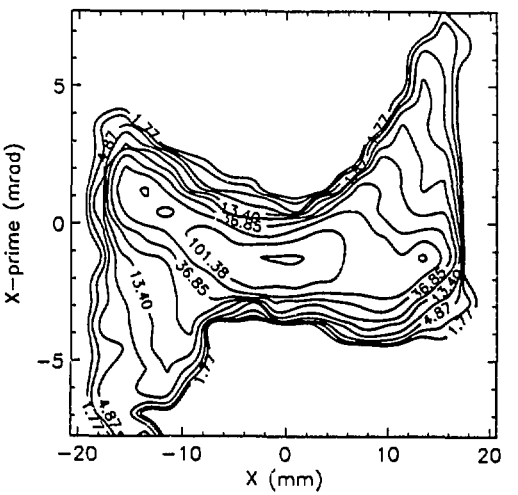

Figure 3: Phase space density contours measured at LP20 for the central longitudinal slice of the 7.4:1 drift compression data.

maximum phase advance variation as

$$\Delta\phi = \int_{LP5}^{LP20} \sqrt{2}\,\sigma_o\, dN \left|\frac{d\beta}{\beta\, dt}\right| \frac{b}{\beta_o c} \approx 0.6\,\text{radians}\,.$$

Here N measures z in lattice periods. Given the relatively rapid (in z) reversal of the beam's compression which limits the communication time, it is unclear whether this effect and the magnitude of mismatch oscillations are sufficient to produce transverse phase space shapes such as Fig. 3.

A second suggested mechanism for emittance growth was the interaction of a compressed (and thus "fat") beam with the small ($\approx$ 10% relative to the quadrupole at the electrode surface) nonlinear dodecapole forces present in the MBE-4 lattice. Previous experiments [2] on MBE-4 have shown that dodecapole-induced phase-mixing for off-axis beams can lead to significant emittance growth. In the present experiments, however, the beam remained within $\approx \pm 0.5$mm of the axis, so simple centroid damping is ruled out. Particle simulation code runs [2] suggest that dodecapole-induced emittance growth will occur for centered, drift-compressed beams with the predicted magnitude sufficient to explain the 3.7:1 compression data. The simulation results are not as clear-cut for the 7.4:1 case, due to difficulties such as particle loss to the walls (which possibly occurred in the experiment also). D. Grote at LLNL (private communication), however, has produced butterfly shapes in a 3D simulation of MBE4 compression including dodecapole forces. Space charge non-uniformities, which appear to be quite important for $z \gtrsim$LP10 in the 7.4:1 data, probably also affected the evolution of the transverse phase space. Such non-uniformities (both symmetric and non-symmetric) can present strong, nonlinear perturbations for highly space-charged depressed beams such as MBE-4.

Summarizing, strong (7.4:1) and rapid compression ($d\lambda/\sigma_o dN \geq 0.1\lambda$) of the MBE-4 beam led to large emittance growth. We believe that the cause is interaction of the outer portions of the beam with nonlinear dodecapole focusing forces and possibly non-uniform space charge distributions. Weaker (3.7:1) and less rapid compression ($d\lambda/\sigma_o dN \leq 0.05\lambda$) showed little or no RMS emittance growth. Most HIF driver designs have $d\lambda/\sigma_o dN \leq 0.005\lambda$ within the accelerator. Hence, non-adiabatic, rapid compression problems, if they occur at all, are far more likely in the final focus section rather than within the accelerator.

References

[1] T. Garvey *et. al.*,"Transverse Emittance Studies of an Induction Accelerator of Heavy Ions", Poster *XRA51*, these proceedings.

[2] S. Eylon *et al.*,"Emitance Variations of Very Cold Ion Beams During Transport Through MBE-4", in *Proc. Int. Symp. on Heavy Ion Inertial Fusion*, Monterey, CA, Dec., 1990, to appear in Part. Accel., 1991.

Low-Emittance Uniform-Density Cs^+ Sources for Heavy Ion Fusion Accelerator Studies*

S. Eylon, E. Henestroza, T. Garvey, R. Johnson and W. Chupp

Lawrence Berkeley Laboratory,
University of California
Berkeley, California 94720

ABSTRACT

Low-emittance (high-brightness) Cs^+ thermionic sources were developed for the heavy ion induction linac experiment MBE-4 at LBL. The MBE-4 linac accelerates four 10 mA beams from 200 keV to 900 keV while amplifying the current up to a factor of nine. Recent studies of the transverse beam dynamics suggested that characteristics of the injector geometry were contributing to the normalized transverse emittance growth. Phase-space and current density distribution measurements of the beam extracted from the injector revealed overfocusing of the outermost rays causing a hollow density profile. We shall report on the performance of a 5 mA scraped beam source (which eliminates the outermost beam rays in the diode) and on the design of an improved 10 mA source. The new source is based on EGUN calculations which indicated that a beam with good emittance and uniform current density could be obtained by modifying the cathode Pierce electrodes and using a spherical emitting surface. The measurements of the beam current density profile on a test stand were found to be in agreement with the numerical simulations.

I. INJECTOR DESCRIPTION AND CHARACTERISTICS

Four 10 mA Cs^+ ion beams are emitted thermionically into the diode gap from alumino-silicate layers coated on molybdenum cups[1]. The cups are mounted on a Pierce shaped graphite plate anode connected to a -200 kV Marx pulse generator. The beams, focused along the diode, pass through four holes in the cathode ground plate into the MBE-4 matching section. The ion source phase-space and current density distributions were determined experimentally using a pinhole and slit combination coupled to a Faraday cup. The pinhole was placed as close as possible to the ion source exit at a position where the beam is still cylindrically symmetric. Figure 1 (lower) shows the agreement between the measured beam phase-space distribution and the result of an ECUN[2] simulation for a zero emittance beam. One can see that the outermost rays of the beam are turned toward the diode axis due to overfocusing as a result of the diode field aberrations. This leads to current accumulation at the beam edges resulting in a hollow beam (figure 2, lower). Recent studies[3] have suggested that the source properties may contribute to the measured emittance growth for the 10 mA accelerated beam. A quick solution to improve the source beam dynamics by scraping the beam current to 5mA was temporarily adopted. Along with this solution we have developed a new improved 10 mA source.

II. THE 5 mA SOURCE

A simple way of eliminating the outermost beam rays is to use a circular aperture ring (scraper) placed at the cathode plate, thus stopping down some of the beam current. Faraday cup measurements of the current taken at the entrance to the MBE-4 matching section initially showed a deteriorated current waveform. This appeared as an increase in the current rise-time and the total beam current. This current increase may be due to additional secondary electrons emitted from the scraper and accelerated towards the anode. To re-capture these secondary electrons the scraper was biased with a positive 4.5 kV d.c. voltage. Beam current waveforms at various bias voltages are shown in Fig. 3. The scraper is recessed 0.8" from the diode exit to eliminate electric field effects due to the bias voltage. The beam phase-space and current density distributions for various scraper diameters (0.4", 0.45", and 0.5") were measured and found to be in agreement with EGUN simulations. An optimum scraper diameter of 0.45" was chosen leading to a current of 4.5 mA and a higher quality beam as shown in Fig. 4. Transverse emittance measurments along MBE-4 using the high quality 4.5 mA beam revealed a normalized transverse r.m.s. emittance of 0.03 mm-mrad, reasonably consistent with the 0.1 eV temperature of the source emitter. Furthermore, the 4.5 mA beam showed a significant reduction in the variations of the measured r.m.s. transverse emittance in the MBE-4 matching section as compared to the 10 mA beam (figure 5).

III. THE 10 mA IMPROVED SOURCE

The new 10mA source consists of a curved ion emitter, a modified Pierce electrode (graphite plate) and a new mechanical assembly. EGUN simulations of the new improved source show a uniform current density and a lower emittance for a beam emerging from the new diode and scraped with a 20 mm aperture to 10mA at the input to the MBE-4 matching section. Improved fabrication techniques were developed and used to produce the new curved emitters. The performance of the new emitters was evaluated in a test stand using a diode configuration with an anode-cathode spacing of 0.5" and voltages up to 20kV. Figure 6 shows a temperature profile taken on the emitter surface along the diameter and Faraday cup current density through crossed slits positioned 0.9" from the cathode grid. The current density measurements were found to be in agreement with EGUN simulations for the

*Work supported by the Office of Energy Research, Office of Basic Energy Sciences, U.S. Department of Energy. Contract DE-AC03-76SF00098.

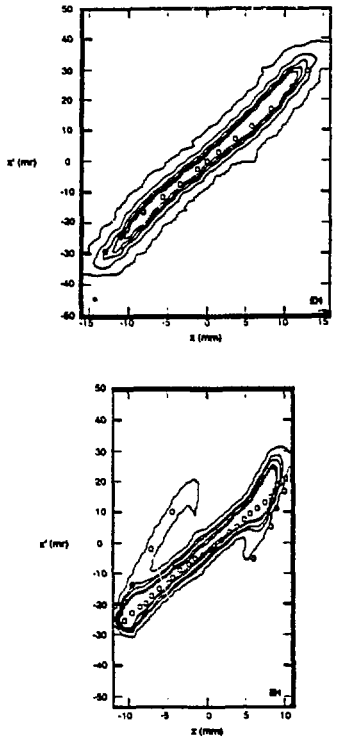

Fig. 1 Measured beam distribution in (x,x') phase space at diode exit. Comparison between experiment (-) and EGUN (o). Upper (lower) figure refers to the new (old) source.

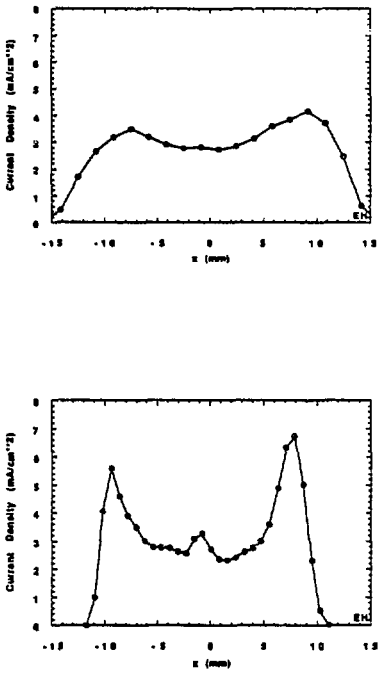

Fig. 2 Measured beam current density distribution vs. radial position. Upper (lower) figure refers to the new (old) source.

same geometry , thus approving the emitter for further tests in the MBE-4 ion source. The new mechanical assembly, which stabilizes the diode geometry (especially when going from air to vacuum) and improves the emitter alignment, was installed in the MBE-4 ion source section. The new mechanical assembly uses four insulating posts connecting the graphite plate (anode) to the output aperture plate (cathode). The mechanical stabilty of the diode was surveyed using optical telescopes placed at the far end of MBE-4 and set to have a line of sight coinciding with the MBE-4 axis. To perform the survey we have replaced the left and right-hand sources with "targets" containing a point source of light. A displacement of less than 0.007" was measured when the system went from air to vacuum. The assembly was tested for high voltage breakdown and found to withstand high voltage pulses in excess of 220 kV and 10 micro-second duration applied between the cathode and anode.

The new curved source was placed at the right-hand beam position and operated to evaluate the diode performance. Close agreement between the measured and the designed diode parameters, as predicted by previous EGUN simulations, was obtained when the source emitting surface was heated up to 1010 ^{o}C. The temperature was measured remotely through a window using a hot wire pyrometer. This temperature was found to be well above the diode current saturation temperature with the diode current determined by Child-Langmuir space-charge limit. The diode current, I_d, was measured for diode voltages, V_d, between ~100kV and ~200kV. The measured diode current was found to follow the well known Child-Langmuir law, $I_d = k\, V_d^{3/2}$, where k is the diode perveance, measured to be 2.3 x 10^{-4} μPervs.

The diode beam dynamics were measured using the aperture-slit technique described earlier. Figure 1 (upper) shows the beam phase-space profile. One can see that the optical

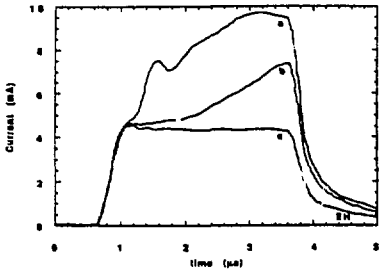

Fig. 3 Scraped beam current vs. time with a scraper bias of (a) 0.75kV, (b) 2.75 kV and (c) 4.75 kV.

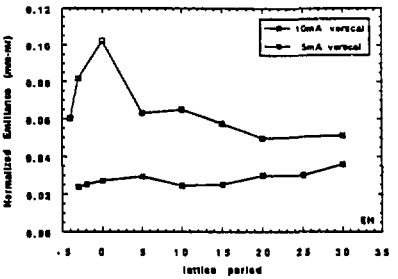

Fig. 5 5 mA and old 10 mA beam r.m.s. normalized transverse emittance vs. lattice period along MBE-4. The matching section corresponds to lattice periods -4 through 0.

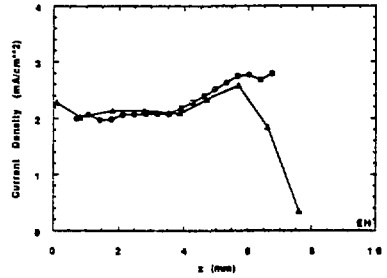

Fig. 4 5 mA beam current density at point of injection into first quadrupole of matching section. Comparison between experiment (Δ) and EGUN code (•).

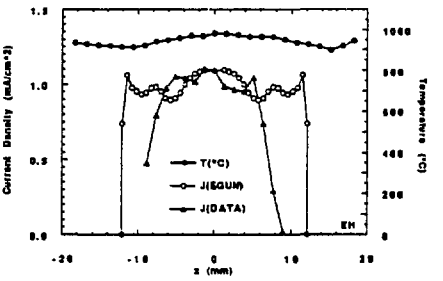

Fig. 6 Test stand measurements of the current density profile J(DATA) compared with EGUN simulation J(EGUN), and the temperature profile taken at the emitter surface.

aberrations in the diode are significantly reduced and that the previous filamentation in the profile is eliminated, thus leading to a more uniform current density profile as shown in Fig. 2 (upper). The full beam current of 16 mA measured using a Faraday cup at the exit of the MBE-4 matching section 1st quadrupole doublet and the beam divergence angle of 30 mrad. taken from the measured phase space profile shown in Fig. 1 (upper) were found to be in good agreement with the parameters predicted by the EGUN simulations. For applications in MBE-4 the beam is apertured to a diameter of 20 mm leading to a beam current of 10.6 mA consistent with the original nominal MBE-4 beam current. The normalized r.m.s. transverse emittance, ε_n, was measured using the double slit technique at the exit of the 1st MBE-4 quadrupole doublet and found to be 0.067 mm-mrad. As the intrinsic emittance of the beam is given by $\varepsilon_n = 2a\,(kT/m_i c^2)^{1/2}$, where m_i is the ion mass, a is the beam radius and T is the beam temperature, we obtain a temperature estimate of 1.4 eV. This is consistent with the source temperature and the adiabatic transverse compression of the beam by the focusing elements. From the measurements of current and emittance we calculate the beam brightness, $I_b/\pi^2\varepsilon_n^2 = 2.4 \times 10^{11}$ A/(m-rad)^2.

ACKNOWLEDGEMENTS

We are indebted to T.J. Fessenden, L. Smith, and A. Faltens for helpful discussions. We thank D. Vanecek for mechanical design effort and W. Tiffany for technical support.

REFERENCES

[1] A.I. Warwick et al, "A four beam cesium injector for MBE-4", IEEE Trans. Nucl. Sci., NS-32, Oct. 1985, pp3196-3198.
[2] W.B. Herrmannsfeldt, "EGUN - An electron optics and gun design program", SLAC Report - 331, October 1988.
[3] H. Meuth et al., "Study of transverse emittance in MBE-4", LBL report, LBL-27230, December 1989.

Survey of Alignment of MBE-4: April 1, 1990 through May 1, 1991

Rudin Johnson, Shmuel Eylon, David Vanecek, Bill Tiffany

Last year we discovered that a focusing imperfection near LP11 in section "C" was "kicking" the beam transversely causing it to oscillate at amplitudes up to 5 mm during transport through MBE-4 [1]. Our initial attempts at locating the source of the difficulty were unsuccessful. To allow the experimental program to continue, Section "F" was installed in place of Section "C"which was placed on a granite machinist flat in our shop to permit a detailed examination. The positions of all the electrostatic quadrupoles in all 4 beam lines were surveyed using newly calibrated alignment telescopes and precision sight level rented from an optical tooling instrument company. We also wanted to evaluate these instruments for potential purchase and use with future experiments.

June 1990: The results of the detailed survey of Section "C" showed that all the quadrupoles were aligned within ±0.004" in all four beam lines. The outside runout with a dial indicator was also checked against the original 06/12/86 assembly measurements. The 1986 runout was ±0.007", but the 1990 measurement yielded only ±0.006". We had expected to find a lateral misalignment 10 times larger. Careful visual inspection of Section "C" showed no obvious loose or damaged structure, except a discoloration at the first accelerating section insulator (inside the vacuum). Section "C" was pumped down and leak-checked but no leaks could be found (even at the point of where discoloration was seen) although a virtual leak could have been present. To permit a more detailed examination of Section "C" the first quadrupole was removed to expose the region where the "kick" was suspected. Again, no large misalignments, damage or looseness could be discovered. Section "C" was then reassembled with a new vacuum seal and placed in MBE-4 where Section "F" had been. In this location a transverse kick will have little effect on the experiments.

July 1990: The entire MBE-4 was surveyed and realigned with Section "F" and Section "C" transposed. We were able to align the accelerator section within ±0.006" both horizontally and vertically. Errors in the matching section were larger, but with the installation of an additional electrostatic steering element at the entrance to the accelerator, the effects of these errors could be corrected and the beams could be centered.

Experience with the improved optical system demonstrated the need for instruments and supports which are both rugged and solid. After gathering information on the latest equipment available, we ordered two line-of-sight telescopes with monofilar reticules and right angle eyepieces, cone type V-block supports, and new sets of 1.5" glass targets [2]. Optical stability of the new system is about ±0.002" horizontally and ±0.004" vertically over the full length of MBE-4 in an 8 hour period. The precision of setting the telescope crosshairs on a lighted target at 50 feet is about ±0.001". MBE-4 experiments ran from July '90 to May '91 without any surveys because the experimental data implied that there were no significant misalignments.

March 1991: The new alignment optics were used to determine movement of the new source installed in March [3]. The source position was determined by light emitting diode targets attached to the source anode structure. The differential movement when going from air to vacuum was reduced from ≈ 0.100" with the old assembly to < 0.015" with the new assembly (better than a factor of 5).

April 30, 1991: After beam tests with the new source were complete, the machine was let up to air and a complete survey of MBE-4 was made. We found no large misalignments of MBE-4. The sections were with ±0.008" of a least squares straight line fit of the beam line, except for the source [Fig. 1].

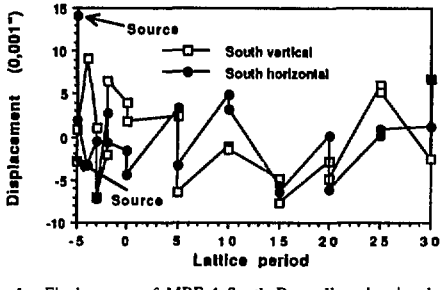

Fig. 1. Final survey of MBE-4 South Beam line showing horizontal and vertical displacements from a least squares straight line fit of survey data.

Bldg. 58 Floor Slab Monitoring Results [4]

The relative position of the Bldg. 58 floor slabs has been monitored on a daily basis for over a year. The direction of movement is what one would expect. There is a motion of the West slab toward the North of 0.020" and hardly any vertical movement (~±0.002") [Fig. 2].

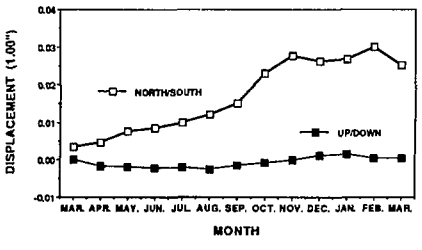

Fig. 2. Average monthly relative movements between the Bldg. 58 floor slabs (from daily readings)

REFERENCES

[1] "Centroid Motion and Transverse Emittance in MBE-4," E. Henestroza, et al., HIFAR Yr. End Report LBL-29743.

[2] "New Optical Survey Equipment for MBE-4," Rudi Johnson, HIFAR Note 302.

[3] "Low Emittance Uniform Density Cs^+ Source for Heavy Ion Fusion Accelerator Studies," LBL-30070a, HIFAN-486.

[4] "Building 58 SLAB Motion," Dave Vanecek, HIFAR Note 299.

Time of flight dependence on the MBE-4 quadrupole voltage.

E. Henestroza, S. Eylon

During our search for a suitable longitudinal accelerating schedule for MBE-4, we have found disagreements between the numerical calculations and measurements of the current waveforms at the diagnostic stations.

The particle-in-cell (PIC) code SLIDE has been used to guide us in our search. Calculations using the old code, SLID, agree with SLIDE calculations when major differences between simulation and measurements have been found. This way we have been able to diagnose several hardware and software problems when running MBE-4.

We have found that the major source of disagreements between the numerical calculations and measurements is in the arrival time of the beam at the different accelerating modules. Since there is a longitudinal electric field along the electrostatic quadrupole doublets, this arrival time will depend on the motion of the beam while crossing the quadrupole channel. We have modeled this acceleration as a double kick located at the center of the quadrupoles (Ref. 1). A schematic view of the MBE-4 lattice layout and the equivalent double kick is shown in Fig. 1.

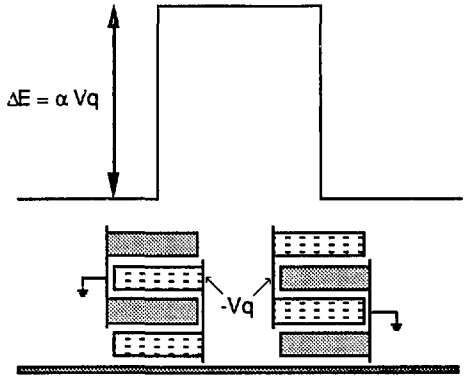

Fig. 1 MBE-4 quadrupole doublet layout and equivalent double kick.

Drift beam time-of-flight measurements along the MBE-4 transport section were performed to obtain the beam arrival time as a function of the quadrupole voltage V_q. A pencil beam was used to minimize longitudinal erosion of the current rise and fall times. The beam arrival time was determined as the difference between the central times of the current waveforms taken at lattice periods 0 and 30 along the MBE-4. Fig. 2 shows the measured beam arrival time dependence on V_q varying from 0.5kV to 22kV keeping the phase advance per period below 90^0.

The above experimental results were used to determine the form factor α defined in Ref.1 and given by:

$$\alpha = -\frac{2L}{s}\frac{E_0}{t_0}\frac{\Delta t}{V_q} = .93 \quad ,$$

were E_0=178.2keV is the beam initial energy, t_0 is the extrapolated time of flight for Vq=0, $\Delta t/V_q$ is the slope of the line in Fig. 2, L=45.72cm is the lattice length and s=17.15cm is the distance between the centers of the quads. Using the above measured form factor in the SLIDE program led to good agreement between the simulation and the measurements of the MBE-4 mild acceleration schedule.

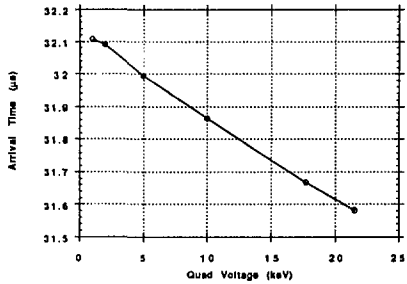

Fig. 2 Measured time-of-flight of a pencil beam between LP0 and LP30 as a function of the quadrupole focusing voltage.

REFERENCES

[1] E. Henestroza, "Longitudinal motion of a beam crossing an electrostatic MBE-4 quadrupole doublet", HIFAR-297.

High Order Calculation of the Multipole Content of Three Dimensional Electrostatic Geometries*

Martin Berz† William M. Fawley and Kyoung Hahn
Lawrence Berkeley Laboratory
University of California
Berkeley, CA 94720, USA

Abstract

We present an accurate and simple method of 3-D multipole decomposition of the field of arbitrary electrode geometries. The induced charge on the surface is obtained by inverting the capacity matrix. The multipole moment decomposition of the resulting potential is readily accomplished using Differential Algebra methodology. The method is applied to the focussing lattice geometry of the MBE-4 accelerator at LBL. Multipole terms of up to the order 5 are computed, and a numerical accuracy of $< 1\%$ is obtained. The effective quadrupole and dodecapole field strength are in good agreement with previous results.

1. INTRODUCTION

In many cases, the exact computation of higher order multipoles in electrostatic geometries is important. For example, in a real quadrupole-focussing geometry, multipole harmonics in addition to the wanted quadrupole one are always present to some degree. The strength of the multipole harmonics depends on the specific geometry of the electrodes, with some harmonics being eliminated or minimized by proper choice of electrode dimensions. The MBE-4, Multiple Beam Experiment at LBL, lattice has many additional multipole components besides the wanted quadrupole component. Although weak, the presence of these components, in conjunction with non-negligible transverse beam displacements, will lead to emittance growth during beam transport[1][2]. To rectify this limitation, we computed the z-dependent strength of the multipole moments using a Differential Algebra (DA) methodology to decompose the three-dimensional focussing potential. The latter is first determined by solving the capacity matrix of the actual electrode and aperture plate geometry. The choice of DA methodology was motivated by its ability to work to arbitrarily high order, with numerical accuracy limited only by that of the capacity matrix. This is in contrast to the more common method of determining the potential on a 3-dimensional mesh, where both the multipole order and numerical accuracy are limited by the mesh resolution. Our calculations show good agreement with previous determinations of the effective quadrupole lengths and dodecapole strengths and we believe that this method may prove useful wherever multipole decomposition of complicated static fields is needed.

2. POTENTIAL PROBLEM SOLUTION BY THE CAPACITY MATRIX METHOD

When a complicated boundary shape is present, a conventional field solver using FFT or SOR techniques becomes computationally expensive because of the large number of mesh points required, especially in 3-D calculations. This difficulty can be alleviated noticeably by calculating the induced charge at the boundary surface directly rather than specifying the field boundary condition. Once the boundary charge distribution is known, the field at the location of a particle can be calculated straightforwardly. Since the number of required mesh nodes is confined to where the actual charges are, *i.e.* at the boundary, substantial reduction in total mesh points is obtained.

In the capacity matrix method, the electrodes are covered with test points $\mathbf{x}_i$ (hereafter called "nodes"). Charge Q_i located at the $\mathbf{x}_i$ are determined such that the potential induced on $\mathbf{x}_i$ by all the other nodes assumes the desired value. This reduces to solving the linear system

$$\phi_j = \sum_i G(\mathbf{x}_i, \mathbf{x}_j) Q_i \qquad (1)$$

where $G(\mathbf{x}_i, \mathbf{x}_j)$ is the Green's function describing the effect of the potential of a charge at $\mathbf{x}_i$ to the point $\mathbf{x}_j$. The inverse to $G(\mathbf{x}_i, \mathbf{x}_j)$ is often called the capacity matrix (C_{ij}). Once the charge Q_i are known, the potential at any point in space can be computed as

$$\phi(\mathbf{x}) = \sum_i G(\mathbf{x}_i, \mathbf{x}) Q_i. \qquad (2)$$

For non-overlapping test charges, one may use the simple Green's function of

$$G(\mathbf{x}_i, \mathbf{x}_j) = \frac{1}{|\mathbf{x}_i - \mathbf{x}_j|} \qquad \text{for} \quad i \neq j. \qquad (3)$$

When computing the self-potential ($i = j$) or when the test charge width σ_i exceeds an internode spacing, the test

*Work supported by the Director, Office of Energy Research, Office of Basic Energy Sciences, Advanced Energy Projects Division, U.S. Dept. of Energy, under Contract No. DE-AC03-76SF00098.

†Presently at Michigan State University

charge profile must be carefully considered. For the 3-D calculations discussed in Sec. 4, a triangular charge distribution was used with

$$\rho(\mathbf{x}) = \begin{cases} \frac{3}{\pi\sigma_i^3}\left(1 - \frac{r_i}{\sigma_i}\right) & \text{if } r_i \le \sigma_i \\ 0 & \text{otherwise} \end{cases} \quad (4)$$

where $r_i = |\mathbf{x} - \mathbf{x}_i|$. With this profile, the potential within σ_i of the test charge is given by

$$\phi(\mathbf{x}) = \frac{Q_i}{\sigma_i}\left[2 - 2\left(\frac{r_i}{\sigma_i}\right)^2 + \left(\frac{r_i}{\sigma_i}\right)^3\right] \quad (5)$$

and

$$C_{ii}^{-1} = \frac{2}{\sigma_i} \quad (6)$$

Although the particular choice of the charge profile is somewhat arbitrary, however, numerical calculations show that the determination of the mutipole harmonics is not highly sensitive to the exact charge profile. The distribution width σ_i is typically set to the internode spacing, depending on the charge distribution used. This choice prevents the self-potential from unphysically dominating the problem. Although we are representing the physically thin surface image charge by non-zero thickness spherical charges, the electric field on and near the beam transport axis should be little affected so long as the internode spacing and charge distribution width σ_i are small compared with the clear aperture between electrodes and the electrode-aperture plate separations in z.

3. MULTIPOLE EXPANSION AND DIFFERENTIAL ALGEBRA

Once the boundary surface charge has been determined (*e.g.* by the capacity matrix method of Sec. 2), the electric potential at arbitrary point in space can be computed by the summation over the charges (see equation (2)). The resulting approximate potential is infinitely differentiable, and thus its Taylor series can be computed. At interior positions where the potential varies smoothly, an approximate functional expansion can prove extremely useful in terms of computational economics. Furthermore, the expansion is quite intuitive because certain nonlinearities of the transfer map couple only with certain multipole terms. For a system such as MBE-4 where the quadrupole moment is by far the dominant component, an expansion around an aperture axis followed by a systematic multipole decomposition of the field is more convenient than the usual power series expansion.

The multipole coefficients $M_{k,l}(z)$ of the potential ϕ are defined in cylindrical coordinates system by

$$\phi(r,\theta,z) = \sum_{k=0}^{\infty}\sum_{l=0}^{\infty} M_{k,l}(z)\, r^k \cos(l\theta) \quad (7)$$

where a Fourier series expansion in θ and power series in r are used. Notice that the up-down symmetry, *i.e.* symmetric under $(y \rightarrow -y)$ transformation, of the MBE-4 geometry is implicitly assumed. No z-axis expansion is performed and $M_{k,l}(z)$ is calculated at numerous locations in z.

The source-free[1] vacuum potential ϕ satisfies the Laplace equation ($\nabla^2\phi = 0$) and thus the $M_{k,l}$ observe the following recursion relation:

$$M_{k,l} = M''_{k-2,l}/(l^2 - k^2), \quad (8)$$

where double prime denotes the second derivative with respect to z. In order that neither ϕ nor $\nabla^2\phi$ be singular at $r = 0$ and that ϕ be bounded at $z = \pm\infty$, the relation $k \ge l \ge 0$ and $k - l = even$ must be true for non-zero coefficients. The entire ensemble of multipole coefficients can then be determined from $M_{k,k}$ and its z-derivatives.

An explicit form for $M_{k,k}$ may be obtained by expressing ϕ as a Taylor series, *i.e.*

$$\phi(x,y,z) = \sum_m \sum_n \frac{x^m y^n}{m!\,n!}\left(\frac{\partial}{\partial x}\right)^m \left(\frac{\partial}{\partial y}\right)^n \phi(0,0,z) \quad (9)$$

After equating this expression with that of eqn. (7) and integrating with $\cos(k\theta)$, one finds for $k \ge 1$

$$M_{k,k}(z) = \sum_{n=0,\ even}^{k} \frac{(-1)^{(n/2)}}{2^{k-1}n!(k-n)!}\left(\frac{\partial}{\partial x}\right)^{(k-n)}\left(\frac{\partial}{\partial y}\right)^n \phi \quad (10)$$

where the up-and-down symmetry has again been used and ϕ is given by the summation over the induced boundary charges,

$$\phi(\mathbf{x}) = \sum_{i=1}^{N} \frac{Q_i}{r_i} \quad (11)$$

Here $r_i \equiv |\mathbf{x} - \mathbf{x}_i|$ and Q_i is the charge at the position of the i^{th} node. Away from the nodes this function is infinitely differentiable, and it is in principle possible (although very tedious for high orders) to compute the required derivatives $M_{k,k}^{(2i)}$ by differentiating expression (10).

To circumvent this difficulty, we use differential algebraic techniques for the computation of the higher order derivatives to machine precision without numerical errors. These techniques, which also play a key role in the high order description of optical systems, have been discussed in detail elsewhere[3][4], and the interested reader is referred to the above mentioned papers.

4. COMPUTATIONAL RESULTS

A FORTRAN code was written to evaluate the $G(\mathbf{x}_i, \mathbf{x}_j)$ of any electrode geometry, and then invert them to obtain the capacity matrix C_{ij} and the node charges Q_i.

In the case of the actual MBE-4 focussing lattice, there are a number of separate elements in the electrode: a)

[1] When beam space charge is present, it is convenient to decompose the total field as a sum of vacuum potential from the boundary charges and the free space potential of the beam charge. Hence, the relevant potential in equation (1) is the *difference* between the specified boundary potential and that due to the beam space charge in the absence of boundaries.

Quadrupole electrodes which are held at either ground or a negative voltage, b) Flat aperture plates from which the electrodes are cantilevered and through whose holes the four ion beams travel, c) A large "can" enclosure surrounding the entire focussing lattice.

The nodes were distributed uniformly over the surface of the electrode rods and with an $\sim 1/r$ dependence on the endplates. The charge distribution width σ_i was set to a constant (≈ 2.5 mm for total node number $N = 5000$), somewhat smaller than the typical internode distance in order to minimize the size effect.

Since our main interest was calculation of three-dimensional multipole components of general potential geometries, the potential at the electrostatic quadrupole electrodes was set to $\pm V_q$ rather than grounding one of the electrode pairs as in the actual case for MBE-4. We have also neglected the "can" enclosure.

In order to evaluate expression (10) numerically, higher order differential algebras were used for the computation of the derivatives of the potential ϕ. From there, the $M_{k,l}$ were computed from 0^{th} to 6^{th} order computed using expression (8).

The coefficients were made dimensionless by scaling the potential by a factor of V_q and using a normalization length of the aperture radius a, *i.e.*:

$$\phi = V_q \sum_{k=0}^{6} \sum_{l=0}^{6} M_{k,l}(z) \left(\frac{r}{a}\right)^k \cos(l\theta) \qquad (12)$$

Figure 1 shows the results for the case of N=5000. Our midplane multipole moments of $M_{2,2} = 0.9855$ and $M_{6,6} = 0.03460$ are in good agreement with 2-dimensional (*i.e.* z-independent) values of 0.9658 and 0.03461 respectively by Brady [5] using POISSON program. Meuth *et al.* [6] experimentally determined an effective quadrupole length of 10.11 ± 0.14 cm by measuring the phase advance of the centroid motion per lattice period(σ_o), 5% shorter than our predicted effective length ($\equiv \int M_{2,2}(z)\,dz \,/\, M_{2,2}(z=0)$) of 10.60 cm (one should note that their most reliable measurement at $\sigma_o = 72°$ gave an effective quadrupole length of 9.99 cm). Our calculation, however, is quite close to the actual electrode length of 10.74 cm.

Near the endplates, the field contains large multipole field components because of the inter-digital structure of the quadrupole rods, their closeness to the endplates, and the beam aperture holes. Our numerical errors may be larger in this region because σ_i exceeds the optimal value around the aperture holes and the spherical charge shape might be a poor approximation to the true image charge distribution on the flat endplates. Thus, perhaps additional nodes and a variable charge distribution width and shape would be required in order to maintain 1% accuracy everywhere.

5. CONCLUSION AND DISCUSSION

We have presented a simple and accurate method of determining the multipole field components of electrostatic focussing system with arbitrary geometry. First the induced surface charge distribution for a given electrode potential is obtained by inverting the capacity matrix, followed by multipole decomposition of the field at the beam axis by using the DA techniques. Since the charge on the conductor surface is calculated directly in this method, the multipole harmonic amplitude can be obtained by the summation of the contributions from all the charges. Although finite size of the charge distribution at a given node poses some uncertainty of the determination of the capacity matrix, the effect can be minimized by optimally choosing the profile shape and width. Numerical experiments show that the decomposition is indeed insensitive to the the charge distribution at the nodes so long as the internode distance is much smaller than the aperture radius.

For the actual MBE-4 accelerator lattice structure, the calculated, z-dependent amplitudes of the multipole harmonics show good agreement with previous measurements in terms of effective quadrupole length and dodecapole strength.

References

[1] C. Celata, I. Haber, L. Laslett, L. Smith and M. Ticfenback, IEEE Trans. on Nucl. Sci. NS-32 (1985) 2480.

[2] S. Eylon, E. Colby, T. Fessenden, T. Garvey, K. Hahn and E. Henestroza, Part. Acc. to be published.

[3] M. Berz, IEEE Trans. Elec. Dev., 35-11 (1988) 2002.

[4] M. Berz, Part. Acc., 24 (1989) 109.

[5] V. Brady, private communication (1987).

[6] H. Meuth, S. Eylon, E. Henestroza and K. Hahn, private communication (1989).

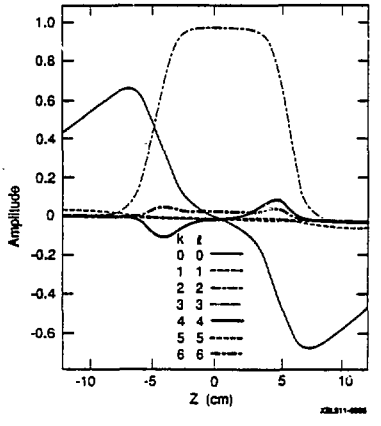

Fig. 1 Multipole decomposition of the MBE-4 lattice plotted versus z for "pure" multipoles $M_{k,k}$.

An Induction Linac Injector for Scaled Experiments*

H.L. Rutkowski, A. Faltens, C. Pike, D. Brodzik, R.M. Johnson, D. Vanecek, and D.W. Hewett**

Lawrence Berkeley Laboratory,
University of California
Berkeley, California 94720

ABSTRACT

An injector is being developed at LBL that would serve as the front end of a scaled induction linac accelerator technology experiment for heavy ion fusion. The ion mass being used is in the range 10-18. It is a multi-beam device intended to accelerate up to 2 MeV with 500 mA in each beam. The first half of the accelerating column has been built and experiments with one carbon beam are underway at the 1 MeV level.

I. INTRODUCTION

The Heavy Ion Fusion Accelerator Research program at LBL is planning to construct an experimental induction linac called ILSE [1] in order to study such phenomena as beam combining, bending of bunches with velocity tilt and pulse compression. In order to build this machine, a multi-beam injector providing ions in the mass range from carbon to potassium and with particle energy for a singly charged ion of about 2 MeV is required. An experimental injector is under construction, however as the ILSE design evolves, its design goals will also evolve. The original design called for sixteen two inch diameter beams providing up to 500 mA of C^+ ions per beam. The design normalized emittance per beam was 5×10^{-7} π m-rad. The high voltage generator, ion source, control system, and the first half of the accelerating column have been constructed and beam experiments at the 1 MeV level are now occurring. We now discuss the existing system and future plans in terms of the three major components:

a) High voltage pulse generator
b) Ion source-extraction system
c) Accelerating column.

II. HIGH VOLTAGE PULSE GENERATOR

This system is an unusual inductively loaded, gas insulated system designed for slow rise long pulse operation. The slow rise time is mandated by the fact that stray capacitances associated with the electrode structure in the column can cause voltage overshoot between gaps when a fast rise pulse is applied. The Marx circuit is loaded by placing one inductor coil in series with the Marx discharge circuit at every other capacitor-spark gap stage. The self inductance of one coil is 18 mh. The full system consists of eighteen plastic trays each containing two capacitors and two spark gaps along with associated charging resistors. The trays hang from a pair of plastic impregnated wood beams inside the pressure vessel which can contain up to 80 psig. of SF_6 gas for insulation. Thus, the structure is modularized and individual trays can be removed for servicing. One coil is mounted around each tray. At the present time, a twelve tray system sufficient for use with the first half column is being used. The same system was used to fire into an open circuit in order to ring the discharge up to 2 MV for a dome-pressure vessel breakdown test. The proper loading of the inductive Marx circuit, to get the desired waveform, is provided by the resistor grading structure on the column itself. This resistor is a double-helix of Tygon tubing filled with conductive water. One leg of the helix runs from ground to the high voltage terminal. The other leg returns back to ground. The conductivity of the $NaSO_4$-water solution in the resistor is controlled by a commercial unit at a level of 27,000 μS for the present configuration. According to circuit simulations, the present system is suited for operation as fast as one shot/5 sec. Normally we use it at 1 shot/10-12 sec for high voltage column conditioning and beam experiments. This rate matches the initial ILSE specification. The purpose of the slower rate is to allow additional pumping to occur inside the column.

One phenomenon observed in the Marx is a reduction of the resistance of the charge resistors with service. The charge resistors are nominally 40 kΩ carbon resistor 1.675" dia. x 12" long rated for 100 W service. These resistors were found to drop in resistance after service in the Marx. Controlled tests showed significant resistance drop when the resistors were subjected to 10 KV pulses of the same shape as the Marx pulse. There is a tendency for the resistance to drop to some asymptotic level after a few pulses and if the voltage of the pulse is increased, the resistance will drop to a new asymptotic level.

The specifications for the high voltage generator are likely to change toward faster rise time, if column stray capacitance will permit, and toward a longer flat voltage duration. Calculations are currently being done to determine if it is possible to reduce the rise time of the pulse applied to the column from the present 30 μsec to ~5 μsec. Finally, we are seeking to increase the rep rate capability of the system to

* Work supported by the Office of Energy Research, Office of Basic Energy Sciences, U.S. Department of Energy. Contract DE-AC03-76SF00098.

** Lawrence Livermore National Laboratory, P.O. Box 808, Livermore, CA 94550

1 Hz. Of course other factors affect the useable rep rate notably the pumping speed of the accelerating column.

III. ION SOURCE AND EXTRACTION SYSTEM

The ions source being used at present is a carbon vacuum arc in conjunction with an electrostatic plasma confinement device (plasma switch) to control emission optics during fast pulse extraction [2]. The carbon arc provides sufficient ion flux for our purposes (>25 mA/cm^2) and in a single charge state [3]. Unfortunately the trigger that initiates the arc discharge does not last more than a few tens of thousands of shots. This is due to the fact that the trigger becomes coated with carbon over time and no remote cleaning technique has proved satisfactory for the long term. It is possible to change from a surface flashover trigger to a gas trigger [4] thus avoiding the carbon coating problem. However, there are other disadvantages to the source, mainly the noisy plasma from the cathode spot.

The ion source has been used together with the plasma switch in a pulsed extraction mode both in the injector itself and in a test stand. The plasma switch voltage is constant for these tests. The plasma switch allows one to extract quiescent beams from the source by electrostatically creating a planar virtual anode layer from which to extract ions. This means that the extraction system does not see the noisy streaming plasma from the cathode spot but rather a layer of ions captured by space charge forces near the plasma switch grid. This advantage of quiescent extraction is affected by the fact that the electric fields around the wires give transverse energy to the ions which ultimately becomes added emittance. Attempts have been made to circumvent this problem by reducing the plasma switch voltage during extraction as suggested by simulation results. The experimental result was that when the plasma switch voltage was reduced, oscillatory pulses were observed in the emittance measuring system and these pulses were not reproducible. Computer simulations were performed to determine whether or not the plasma drift velocity which was known to exceed the Bohm velocity by ~2 was responsible for this behavior. The simulations showed that the equilibrium near the switch changed but was not unstable The most probable explanation for the beam noise is that making the plasma switch transparent by lowering its voltage causes the extractor to use the noisy streaming plasma emitted directly from the arc because the virtual anode layer is quickly destroyed when the plasma switch voltage is dropped. This technique for reducing grid induced emittance may still work if a quiescent plasma is available for the plasma switch.

If a quiescent plasma is available the switch would be used for D.C. shutoff of the plasma from the extraction gap. When the voltage is reduced extraction would occur from the plasma behind the switch. Simulation indicates that the extraction surface should remain very close to the switch grid thus preserving the geometry of the emission surface during pulsed extraction. We are presently constructing a 25 cm dia. cusp field source which would use RF power to generate neon ions. This source is capable of generating up to 10 cm dia. beams which are of interest to the ILSE designers so that higher linear charge density can be generated in the beam. The gas will be admitted to the cusp chamber using a piezoelectric puff valve to reduce the acceleration column gas load. If, for some reason, the concept of reducing emittance generation by modulating the voltage on the plasma switch fails, the cusp field source would be usable for direct extraction of long pulses. If this approach is used, some way of selectively switching the output pulse of the injector must be found.

Meanwhile we continue to use the arc source-D.C. plasma switch combination for tests of the injector first half column. The inherent source emittance available is 2-2.5 x 10^{-6} π m-rad. No further development of the arc source is anticipated because of the perceived advantages of the cusp field source in extending lifetime, use of inert gases, and plasma quiescence.

IV. ACCELERATING COLUMN

The first half of the accelerating column is designed for service at 944 KV. A drawing of the whole assembly complete with ion source and plasma switch is shown in Fig. 1. The cross hatched area represents the beam envelope as calculated with the EGUN [5] computer code for the case of 500 mA C^+ ions and full column voltage. The electrodes in the column are constructed of 6Al4V titanium. The ion source is located on the left. The plasma drifts from the arc cathode to the plasma switch which is operated at -55 V D.C. The 1 cm gap to the right is called the current valve. It is connected to a pulse line which pulses the source positively to inject a 1 μsec pulse into the column at the peak of the Marx voltage pulse. At the output end of the column a long tube (3") is biased at -3 kv with respect to ground to keep electrons generated by background gas ionization from entering the exit of the column and being accelerated toward the source.

The column has been operated to 10% above full design voltage without beam. In the beam extraction mode the column was first used for long pulse extraction directly from the source. For these experiments, the current valve was removed and the plasma switch grid was moved forward to the normal position of the current valve grid. The rest of the source assembly was moved forward by the same amount. The geometry makes it impossible to extract full current (500 mA) into the column and the EGUN predicted value is ~300 mA at full voltage. The measured current with a 4" diameter deep Faraday cup was 210-230 mA. Emittance measurements to study the optics of the beam were undertaken and the results were in good agreement with EGUN. The fact that such long current pulses at full column voltage could be transported reliably is very encouraging.

Experiments are now underway to use the current valve pulser to inject into the column. The voltage pulse is variable from 5-14 KV depending on the charge voltage of the pulse line. The voltage pulse remains unloaded by the presence of the source discharge and shows no pulse distortion. This behavior remains consistent for a full range of delays between the arc

discharge and the current valve pulse. Control of the delay is maintained when the injector is fired as is evidenced by fibre optic monitors of the in-dome pulsers.

Initial experiments with the large aperture Faraday cup revealed a slow leakage current following the Marx voltage pulse and a noisy pulse at the time of the current valve discharge. This was verified to not be electromagnetic noise. After trying many Faraday cup variations a fast response current transformer was installed at the beam exit which verified the final Faraday cup results that net electron current was exiting the column.

Experiments using a current transformer installed inside the column at the current valve exit verified that a noisy ion current pulse was entering the column. Increasing the rise time of the pulse from the initial 300 ns has showed an improvement trend. The current valve diode in 9.75 mm wide. Therefore a 300 ns rise time corresponds to several ion transit times across the gap at the design voltage of 13.6 KV for 500 mA of C^+ ions. The rise time of the pulser had to be increased to 1.5 μsec before a reasonably clean current pulse could be obtained. Tests using this new pulse shape are underway.

REFERENCES

[1] Induction Linac Systems Experiments, Conceptual Engineering Design Study, Lawrence Berkeley Laboratory, March 1989, PUB-5219.

[2] H.L. Rutkowski, R.M. Johnson, W.G. Greenway, M.A. Gross, D.W. Hewett, S. Humphries Jr., Review of Sci. Inst. 61, p. 553, January 1990.

[3] S. Humphries Jr. and H. Rutkowski, J. Appl. Phys. 67, p. 3223, April 1, 1990.

[4] S. Humphries Jr., private communication.

[5] W.B. Herrmannsfeldt, Electron Trajectory Program, SLAC-226, November 1979.

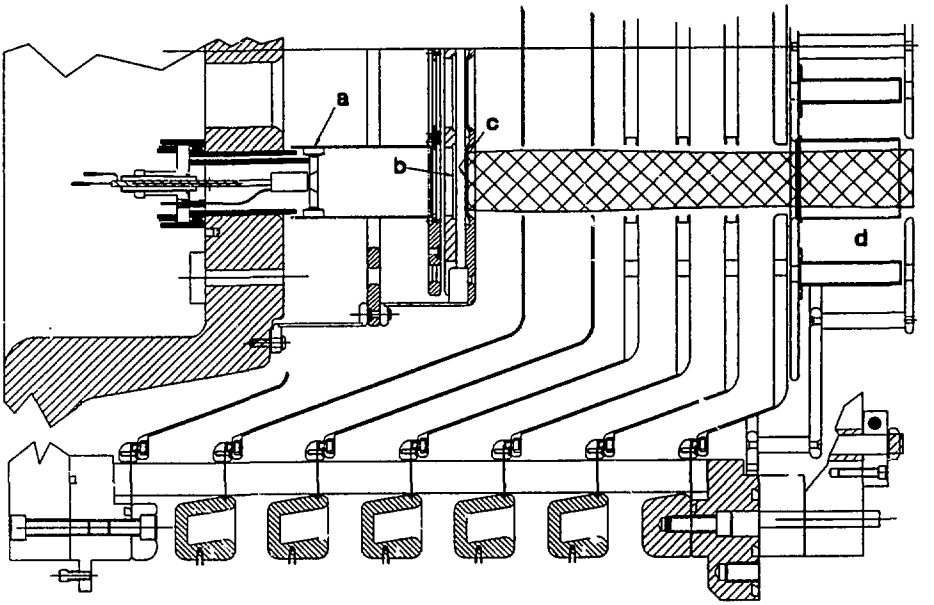

Fig. 1. First half of the full 2 MV injector accelerating column showing a) ion source, b) plasma switch grid, c) current valve grid, d) electron trap. Crosshatched area is calculated beam envelope for 500 mA, C^+ ions at full column voltage.

Induction Accelerator Test Module for HIF*

Andris Faltens

Lawrence Berkeley Laboratory
University of California
Berkeley, California 94720

ABSTRACT

An inducton linac test module suitable for investigating the drive requirements and the longitudinal coupling impedance of a high-power ion induction linac has been constructed by the Heavy Ion Fusion (HIF) group at LBL. The induction linac heavy ion driver for inertial confinement fusion (ICF) as presently envisioned uses multiple parallel beams which are transported in separate focusing channels but accelerated together in the induction modules. The resulting induction modules consequently have large beam apertures-1-2 meters in diameter- and correspondingly large ouside diameters. The module geometry is related to a low-frequency "gap capacity" and high-frequency structural resonances, which are affected by the magnetic core loading and the module pulser impedance. A description of the test module and preliminary results are presented.

I. INTRODUCTION

The induction linac heavy ion driver uses multiple parallel beams which are transported in individual focusing channels but accelerated together in common induction modules. Because the focusing and acceleration requirements change with energy, there is a slow change in the appearance of the accelerator with distance. In the low energy end the preferred scenario is a large number of electrostatically focused beams (e.g. 64) whose quadrupoles occupy most of the available axial space, and consequently the induction cores must surround the cluster of focusing elements, which has a diameter of about 1 m. As the ions gain energy, it becomes more economical to combine the beams to a smaller number of beams (e.g. 16) focused with superconducting magnetic quadrupoles. The diameter of the cluster of quads increases to about 2 m. This transition point is dictated by economics, and nominally takes place at 100 MeV. With further acceleration it becomes advantageous to change to an arrangement where the induction modules alternate with the quadrupole arrays, and the cluster of beams and the resultant module inner diameter can both be reduced back towards the 1 m diameter size. Viewed along the length of the accelerator, the inner diameter would be constant for the first few hundred meters, then bulge out to about twice its initial value, and then gradually decrease. There is a similar variation in the induction core size of the modules, dictated by economics considerations combined with other constraints. At the low energy end acceleration is limited by an assumed velocity tilt limit, which leads to a rapidly increasing allowed acceleration rate with distance, and an increasing core size. Later in the acceleration process, the decrease of pulse duration and maximum electric field limits lead to a decrease of the required core. The resulting outer diameter of the induction cores is about 2 m at the front end, reaches a maximum of about 3 m past the electric to magnetic focusing transition point, and gradually decreases to about 2 m at the end of the accelerator.

II. MODULE CONSTRUCTION

A large induction module which is representative of the required driver modules has been constructed at LBL. The main difference from previous electron and ion induction accelerator modules is the very large central aperture. The test module was made with a 1 m diameter aperture and a 2 m outer diameter. The area which would normally be filled with ferromagnetic core is filled to only a 10% occupancy by winding the core loosely and by alternating thin spools of tape of about 1 cm radial buildup with empty regions of about 9 cm radial extent. This choice of geometry allows the high power measurements to be performed at a relatively comfortable level of 20 kV or less, and allows probing the voltages and currents within the core region, whereas a completely filled core would require up to 200 kV for the same measurements. Figure 1 is a photograph of the module near the completion of its assembly. The largest conveniently available insulator, shown in the middle of the picture, has a diameter of 0.7 m, but the other important dimensions are full size. The top surface of the module, which is not yet installed in the photograph, has an array of capacitive dividers and current loops which enable the voltage and current distributions to be measured in the "gap" region of the induction module. The bottom plate has a similar array of probes, some of which are visible in Fig.1. The intermediate plate, 25% of which is shown in the photo, has provisions for single, two-point, and three-point drive connections at its outer radius. The spaces between spools of tape are largely filled with aluminum ducting to approximately maintain the capacitance of a solid core. The same effect could have been achieved by winding the core loosely.

The core is wound from Metglas 2605 CO material insulated with SiO_2 microspheres and the transformer oil into which the core is immersed. This insulation combination has been satisfactory for core switching speeds of 1 μs and above for the 5 cm wide, 25 μm thick ribbon used. For shorter pulse durations and dense packing the preferred insulation today would be interleaved thin mylar. The tape was rewound from 0.36 m diameter spools onto 12 spools of diameters ranging from 1 - 2 meters, without subsequent annealing. The 2605 CO material was chosen because it has low sensitivity to stress on its magnetic properties. The spools of tape are arranged in 6 sections radially and 2 sections axially. The

* Work supported by the Office of Energy Research, Office of Basic Energy Sciences, U.S. Department of Energy. Contract DE-AC03-76SF00098.

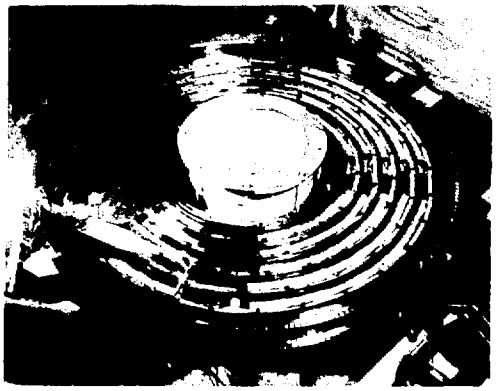

Fig. 1. The induction accelerator test module.

excitation winding is formed by joining the intermediate plate to the bottom plate with a copper cylinder. The external drive is applied at one or more discrete points at the outer radius.

III. MODULE ISSUES, MODELS, AND MEASUREMENTS

The issues which the test module is intended to address are the drive power requirements for the various pulse durations of interest, the drive pulse transients, the beam loading transients, and the longitudinal coupling impedance presented by the module to the ion beam. There has been an upsurge of interest in the longitudinal coupling impedance due to high-frequency cavity modes in the past year or so, and the initial measurements have consequently concentrated on this topic. The transverse coupling impedance and the beam deflections induced by the drive current are lesser concerns. A practical question is whether the module geometry needs to be modified for driver designs to reduce the Qs of higher order mode resonances, or whether the Qs are low enough without additional attention. In the present and ensuing discussion various common terms such as voltage, current, Q, and impedance are used in their customary senses even though they are applied to an intrinsically nonlinear and time-dependent induction device. Use of the familiar cavity mode designations such as TM010, TM110, etc., however, is inaccurate and misleading, because these usually refer to oscillations in a pillbox cavity with short-circuit boundary conditions at the outer radius, whereas the induction cavities have a complicated impedance boundary at the outer radius which is closer to an open circuit.

The uncertainties in the electrical operation of an induction module arise largely from the induction core. In the usual operating sequence, a reset pulse is used to saturate the core material in the reverse direction and then leave the core at the remanent magnetization level. In some cases the reset current flows through the core while the drive pulse is applied. In either case, the drive pulse is very much larger than the reset pulse, and depending on the desired pulse duration, drives the core close to or into complete saturation in the opposite sense on a time scale of a microsecond or so. One of the goals is to eventually determine the rf properties of the module during this switching process. Except for the faster time scale involved, this is essentially the same process that takes place in the ferrite-tuned rf acceleration cavities used in synchrotrons. The major difference is that the rf modes of an induction cavity play no useful role in the acceleration process and are instead the analogues of parasitic resonances in a pulse transformer. In the preliminary measurements reported here, the rf and drive pulses are applied separately, but the rf can be applied at various static states of core magnetization.

Ideally, an induction module would have a core with such a high impedance that it could be replaced with an open circuit; the resulting geometry is two "washers" facing each other and connected through a pulse generator with impedance, Rg, as shown in Figure 2. This geometry is needed partly to provide an acceptable electric field distribution in the vicinity of the beams, and partly to shield the beams from possible deflections from the core drive current. At low frequencies the equivalent circuit is the generator in parallel with a capacity, the "gap capacity" formed by these washers, where it is understood that the electric fields are confined to the interior of the structure. At higher frequencies, the first important resonances are the various ring modes of the structure, which are essentially TEM-like waves running circumferentially around the structure. Their character depends on the relative magnitudes of the characteristic impedance of the stripline formed by the washers and the drive or generator impedance. If the generator impedance is low compared to the line impedance, as might be the case for a very high current accelerator, then the lowest mode is a quarter-wave oscillation, where distance is measured from the drive point to the open circuit symmetry point opposite, followed by the $3\lambda/4$, $5\lambda/4$, etc. modes. If the opposite impedance ratio holds, then the lowest mode is a half-wave oscillation, followed by the λ, $3\lambda/2$, etc. modes. The electrical length of the structure is well approximated by measuring distance at the average radius of the washers. A comparison of the calculated and measured resonant frequencies is given in Fig.3. Relation of these resonances to a coupling impedance depends on the particle velocity, the beamlet arrangement, and the mode of oscillation among the beamlets. This will be the subject of a future publication. There is not a clear distincton between deflecting and accelerating modes as in a single beam machine with high-Q rf cavities, because what is a deflecting cavity mode for one beamlet mode of oscillation can be a longitudinal cavity mode for another beamlet mode of oscillation. Also, because these modes are incidental to the operation of the linac, the radial and

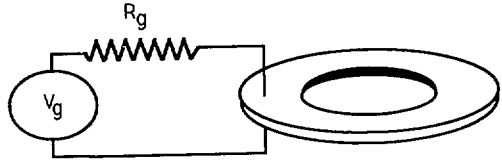

Fig. 2. The circuit idealization for the module.

axial transit time factors can be made very low if desired without affecting the basic acceleration mechanism. A reasonable algorithm is to average the central electric field distribution over the beamlet mode of oscillation; for example, the 0 or in-phase mode of the beams would not interact longitudinally with any of the azimuthally varying electrical modes which have an integral number of wavelengths circumferentially, but would have a transverse coupling impedance, whereas a mode of oscillation where the beams are out of phase across a diameter would have a longitudinal coupling impedance as well as a transverse impedance from the full wavelength mode. Most of these modes have the beams passing through the low-amplitude portions of their fields and therefore have low coupling impedances.

At higher frequencies, the azimuthally symmetric modes begin to appear. For a drive impedance which is high compared to the mode characteristic impedance, the lowest one of these is the analogue of a radial half-wave mode. Beginning with an open circuit at the outer radius, the mode can be computed by making an impedance transformation to an open circuit at zero radius. A conceptual simplification is to taper the radial lines slightly to counteract the impedance change with radius of the parallel plate geometry, in which case the radial extent of the plates is a free-space half-wave shortened by the index of refraction. Although tapered plates are an option for the modules because of their mechanical strength, most similar modules have been constructed in a planar geometry, as has been the test module, and this has the effect of lowering the lowest resonant frequency by about 30%. With a tapered geometry and the assumption that the drive impedance can be averaged over the outer circumference, the impedance at these resonances is the drive or generator impedance. If the geometry is not tapered, but the generator impedance is spread over the outer circumference, then the coupling impedance rises with frequency, eventually by a factor of Ro/Ri, which is a factor of two for the test module. In the actual geometry of a discrete number of drive points, there is no easy simplification that is useful for the required impedance transformation from the drive terminals to the center of the module, but a measurement is very easy.

The presence of the induction core and the necessity to enclose it with a conductor perturbs the frequencies of the previously described simplified modes and, together with the generator impedance determines the Qs of the resonances. The core winding conductor introduces a zero in the impedance at zero frequency, followed by a pole or impedance peak at about 10 MHz, which is the lumped element parallel resonance of the gap capacity and the core inductance. The inductance and damping are expected to vary during the acceleration pulse because of the changing state of magnetization of the core material, and if it is similar to the much more familiar case of ferrite its properties will be a function of the amplitude of the rf excitation. The losses are expected to increase with amplitude. For the low frequency lumped element resonance, the beam coupling impedance is dominated by the module generator impedance and is limited to a low value. For the higher-frequency higher order modes, the damping from the core material is expected to be more important. At low amplitude and in a static magnetization condition, the Qs of the resonances are near 10, as shown in Fig.3. Further measurements will look at the amplitude dependence of these same resonances and their dependence on the dynamic magnetization process. The apparatus for these more extensive measurements has been acquired. The measurements reported here are the first results of a more comprehensive program planned for the remainder of this year.

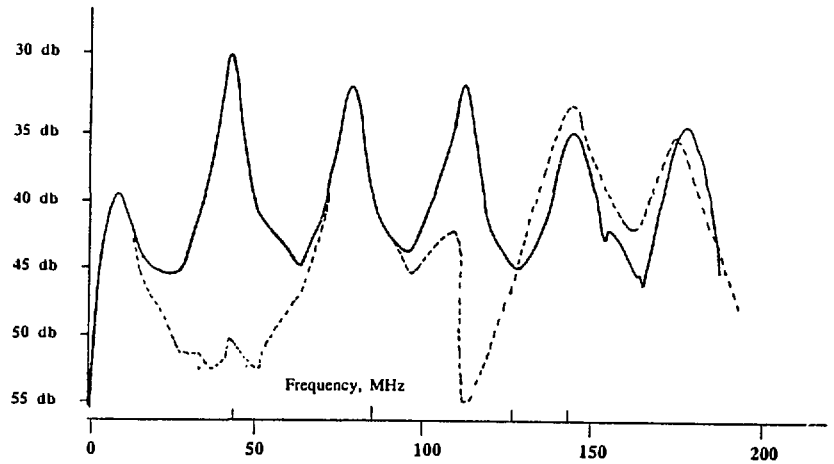

Fig. 3. Transmission measurements to a diametrically opposite voltage pickup,solid curve and ∘ pickup near 90°, dashed curve, from a high impedance drive point. The first resonance, f ≈ 10 MHz, Q ≈ 1, is the lumped element LC parallel resonance of the module. The next set of resonances is the circumferential or ring modes, f ≈ 42 MHz, 80 MHz, etc., Q ≈ 10. Alternate resonances of this set have a voltage null near the 90° pickup, seen in the dashed curve, which aids in identifying these modes. The radial modes become evident beyond 140 MHz and have lower Q's. The resonant frequencies calculated for the simplified models are 42, 84, and 126 MHz for the ring modes and 142, 226 MHz for the radial modes, which are indicated by the marks on the frequency scale.

Longitudinal Instability in HIF Beams*

Lloyd Smith

Lawrence Berkeley Laboratory,
University of California
Berkeley, California 94720

ABSTRACT

In contrast to an electron induction accelerator, in which the particle velocity is virtually constant, the resistive and inductive components of accelerating module impedances can cause instability for an intense non-relativistic heavy ion beam accelerated in a similar structure. Since focusing requirements at the fusion pellet imply a momentum spread $\lesssim 3\times10^{-4}$ at the end of the accelerator, it is essential to understand and suppress this instability. There is also an economic issue involved for this application; selection of parameters to control the instability must not unduly affect the efficiency and cost of the accelerator. This paper will present the results of analytic and computational work on module impedances, growth rates and feed back (forward) systems.

I. INTRODUCTION

Inertial Confinement Fusion is based on the concept of creating a condition of very high density and temperature in a fuel pellet a few millimeters in size for a few nano-seconds. The material is not confined by external forces; the finite reaction time is due to the inertia of the fuel as it flies apart. For this process to work, an energy of several megajoules must be deposited in a thin surface layer in a few nano-seconds-an instantaneous power requirement of several hundred terawatts. The candidates for delivering the energy are lasers, which can deliver the required power but are as yet deficient in total energy and desired repetition rates of a few per second, and particle accelerators, which can deliver the required energy at a good repetition rate but as yet not at the required power level. Because the stopping distance is set by the required thickness of the surface layer, the choices in particle beams range from millions of amperes of light ions at several MeV kinetic energy to thousand of amperes of heavy ions at several GeV kinetic energy. At the heavy ion end of the scale the candidates are a set of R-F linacs plus accumulation and storage rings to reach the required level of joules and watts, and a linear induction accelerator, which is capable of accelerating kiloamperes of beam and would deliver the required energy and power in a single shot. The subject of this paper is a longitudinal instability which is certain to occur in an induction linac and is currently considered to be a major question as to the feasibility of the induction linac option.

Work supported by the Office of Energy Research, Office of Basic Energy Sciences, U.S. Department of Energy. Contract DE-AC03-76SF00098.

II. THE PROBLEM

The instability in question is a close relative of the well-known microwave instability in circular accelerators but with distinctive features in this unfamiliar parameter range. That it should occur in a linear accelerator is due to the fact the ions are non-relativistic all the way (10 GeV at mass 200 → 50 MeV/nucleon → $\beta = 0.3$) and regenerative bunching can occur at an unpleasant rate in a kilo-ampere beam subjected to the impedance of the accelerating modules themselves.

Figure 1 shows a typical module as presently conceived. The module is energized through the transmission line entering at the upper left; the characteristic impedance of this line is seen as a resistance by the beam. Analytic estimates, more or less corroborated by model measurements, indicate that in the frequency range of greatest concern, about five to fifty megahertz, the impedance is well represented by a parallel R-C circuit–the line impedance in parallel with the capacity of the narrow gap below the end of the feed line. At about 100 MHz, there are modes involving the space above the magnetic material to the right of the transmission line which can be represented by a parallel R,L,C circuit. Unfortunately, the Q of this mode depends on R-F properties of the magnetic

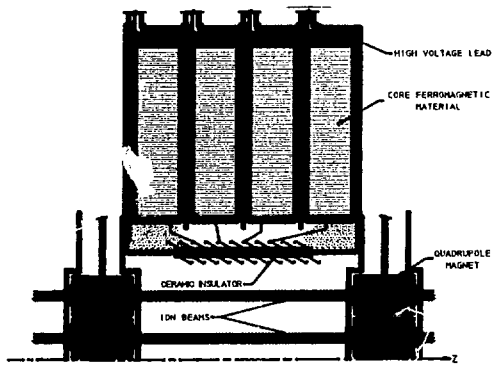

Fig. 1. Typical set of accelerating modules. The voltage is applied through the leads at the top and appears across an insulated gap below the leads. The insulating material can be seen projecting into the space below the magnetic material.

material, probably Metglas, which are not known at this time. Finally, there are many modes at much higher frequency associated with the pill-box like region surrounding the beam, but those are thought to be unimportant. In fact, PIC simulations indicate that even the 100 MHz mode is only marginally important.

The low frequency impedance is, however, quite important and here arises a conflict with the over-all performance and cost. To ease the instability, the line impedance should be as low as possible and the gap capacity as high as possible to shunt the R-F image currents away from the resistance. These desires are diametrically opposed to the demand for high efficiency and low cost. Maximum efficiency requires that the line impedance be equal to the module voltage divided by beam current to maximize reflected power. Also, the characteristic time $\tau = RC$ should be short compared to the beam passage time of 100-500 ns. in order to establish the required voltage without undue strain–i.e., the capacity should be low. As will be seen in the next section, best performance and cost lead to a predicted e-folding distance of about 100 meters in an accelerator five to ten kilometers long. In order to bring the theoretical problem into a range of control by momentum spread (less than $\sim 3\times10^{-4}$ because of chromatic effects in focusing on the fuel pellet) and/or feed-forward (see later section) we contemplate reducing line impedance by a factor of three (25% efficiency loss) and increasing the RC time by a factor of three (cost unknown).

III. THEORY

Instead of working with the Vlasov equation, it is simpler to work with the linearized fluid equations with zero pressure (no momentum spread), keeping in mind that the criterion for stabilization by a momentum spread is the same as for the microwave unstability of a coasting beam. Furthermore, the situation is formally similar to the transverse beam break-up instability without an external focusing force and will be analyzed in a similar fashion. The fluid equations are:

$$\frac{\partial}{\partial t}\frac{1}{v} + \frac{\partial I}{\partial z} = 0 \qquad \text{continuity equation} \qquad (1)$$

$$\frac{\partial v}{\partial t} + v_0\frac{\partial v}{\partial z} = \frac{eE}{m} - \frac{eg}{4\pi\varepsilon_0 mN}\frac{\partial}{\partial z}\frac{I}{v} \qquad \text{Force equation} \qquad (2)$$

$$\frac{\partial E}{\partial t} + \frac{E}{\tau} = -\frac{1}{C}(I-I_0) \qquad \text{Circuit equation} \qquad (3)$$

where I is current, v is velocity, and I_0 and v_0 are the unperturbed values.* C is the capacity, averaged in z, in Farad-meters of the low-frequency equivalent circuit, R is the smoothed resistance in ohms/meter, τ=RC, and N is the number of beamlets simultaneously accelerated.

The second term in (2) is the space charge force per beamlet since the beamlets are isolated transversely by closely spaced conducting sheets inserted in the beam region of Fig. 1. It has the effect of producing space charge waves running forward and backward along the beamlets. As the accelerator was first conceived, there was to be a single beam (N=1) and stability seemed to be insured by the mechanism that backward moving waves growing amplitude would reflect from the back end of the bunch and damp out as they moved forward. In the present concept there would be a dozen or more separate beamlets. The space charge force is then negligible compared to the induced module force in the low frequency range and will be omitted hereafter.

If time is replaced by $t - z/v_0$, the time after the head of the bunch passes a particular point along the accelerator, the equations become:

$$v_0\frac{\partial}{\partial z}\frac{\delta I}{I_0} = \frac{\partial}{\partial t}\left(\frac{\delta v}{v_0}\right) \qquad (1')$$

$$\frac{\partial}{\partial z}\frac{\delta v}{v_0} = \mathcal{E} \qquad (2')$$

$$\frac{\partial \mathcal{E}}{\partial t} + \frac{\mathcal{E}}{\tau} = -K^2 v_0\frac{\delta I}{I_0} \qquad (3')$$

where $\mathcal{E} = \frac{e\delta E}{mv_0^2}$ and $K^2 = \frac{eI_0}{mv_0^3 C} = \frac{eI_0 R}{mv_0^3\tau}$

The most likely way for a perturbation to be launched is by a voltage error on a module at (say) z=0. The initial conditions for the set of equations are then:

$$\frac{\delta v}{v_0}(0,t) = f(t)$$

$$\frac{\delta I}{I_0}(0,t) = 0 \qquad (4)$$

$$\mathcal{E}(0,t) = \mathcal{E}(z,0) = 0$$

Using a Laplace transform in z:

$$\tilde{y}(k) = \int_0^\infty dz e^{-kz} y(z) \quad , \qquad (5)$$

the equations lead to

$$\hat{\mathcal{E}} = -\frac{K^2}{k^7+K^2}\int_0^t dt'\frac{d}{dt'}f(t')\exp\left[-\frac{k^2}{k^2+K^2}\frac{t-t'}{\tau}\right] \qquad (6)$$

* This analysis neglects acceleration; the qualitative features are not seriously affected by this omission.

If the initial velocity perturbation is $\frac{\delta v}{v_0} = \Delta e^{i\omega t}$, the integral in (6) is easily done and the Laplace transform can be inverted analytically or by a numerical integration around the poles. The analytic result is:

$$\mathcal{E} = -\frac{K\Delta e^{-t/\tau}}{1+i\omega\tau}\left\{\sum_{n=0}^{\infty}\frac{(Kz)^{n+1}j_n(Kz)}{n!^2}\left(\frac{t}{2\tau}\right)^n + i\omega\tau\sum_{n=0}^{\infty}\frac{1}{n!}\left(\frac{t}{\tau}\right)^n\sum_{k=0}^{n}\frac{(Kz)^{k+1}j_k(Kz)}{2^k k!}(1+i\omega\tau)^{n-k}\right\} \quad (7)$$

where $j_n(Kz)$ is the n^{th} order spherical Bessel function.

Figure 2 shows two examples of the corresponding $\frac{\delta v}{v_0}$ as a function of Kz and t/τ. The most violent growth occurs for $\omega\tau = \frac{1}{\sqrt{3}}$ but becomes relatively benign for higher frequencies; the case, $\omega\tau=3$, is also shown for comparison.

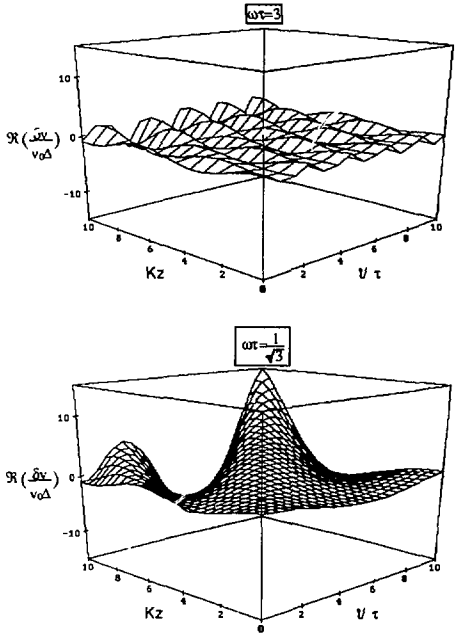

Fig. 2. $\frac{\delta v}{v_0\Delta}$ as a function of Kz and t/τ for $\omega\tau = 3$(top) and $\frac{1}{\sqrt{3}}$ (bottom). Kz = 10 corresponds typically to a distance of one to three kilometers.

Equation (7) is not very revealing of essential features, which can be seen better by setting $\frac{df}{dt} = \delta(t)$ in equation (6) and using a saddle point analysis.[1].

The inversion integral becomes:

$$\mathcal{E}(z,t) = \frac{K^2}{2\pi i}\int\frac{dk}{k^2+K^2}\exp\left[kz - \frac{k^2}{k^2+K^2}\frac{t}{\tau}\right] \quad (8)$$

The method of steepest descents consists in finding the stationary points of the quantity in the exponent by setting its derivative equal to zero and then integrating across these saddle points to approximate the contour integral. Our interest, however, is only in the real part of the exponential at the saddle points; that is, the real parts of the solutions to the equation:

$$\frac{d}{du}\left[uKz - \frac{u^2}{u^2+1}\frac{t}{\tau}\right] = Kz - \frac{2u}{(u^2+1)^2}\frac{t}{\tau} = 0 \quad (9)$$

The roots of the quartic depend on the ratio $\frac{t}{\tau Kz}$. A case of particular interest [1] is when $\frac{t}{\tau} < \frac{8}{3\sqrt{3}}Kz$. The real part of the exponent is then given by:

$$Kz\left\{u - \Delta + \frac{2u\Delta^2}{\Delta^2+16\mu^4\left[1+\mu^2-2\mu\sqrt{1+\mu^2}\right]}\right\} \quad (10)$$

where $\Delta = t/\tau Kz$ and μ is defined by $\Delta = 4\mu^2\sqrt{1+\mu^2}$. The bracket is a maximum at $\Delta = \frac{3}{4\sqrt{2}}$, where (10) becomes $\frac{Kz}{2\sqrt{2}}$. That e-folding rate is the same as the worst case $\omega\tau = \frac{1}{\sqrt{3}}$ shown in Fig. 2. The point of maximum growth should move backward along the bunch at $\frac{t}{\tau} = \frac{3}{4\sqrt{3}}Kz$, in rough agreement with Fig. 2.

Numerical Values

For $\omega\tau = \frac{1}{\sqrt{3}}$, the frequency is $f = \frac{1}{2\pi\sqrt{3}\tau} = \frac{1}{2\pi\sqrt{3}}\frac{t_p}{\tau}$,

where t_p is the pulse duration. For the desirable value, $\frac{t_p}{\tau} \sim 20$, f = 4-20 MHz for t_p = 500-100 n.s. and f = 1-7 MHz for τ increased by a factor of three. These frequencies are well in the range of the R-C model. The growth rate is $\frac{K}{2\sqrt{2}} = \sqrt{\frac{el_0R}{16W\ell_p}\frac{t_p}{\tau}}$, where W is the kinetic energy and $\ell_p \sim$ 10 meters, is the bunch length. If the module feed line is matched, el_0R = 1 MeV/meter, the intended acceleration rate.

Then for W = 1 GeV and $\frac{t_p}{\tau} = 20$, $\frac{K}{2\sqrt{2}} \sim (100 \text{ meters})^{-1}$. If R is reduced by a factor of three and τ increased by a factor of three, $\frac{K}{2\sqrt{2}} \sim (300 \text{ meters})^{-1}$.

Feed Forward

Since the ions are non-relativistic ($\beta < 0.3$), the possibility arises of observing some aspect of the unstable growth at one point along the accelerator and preparing a down stream module to apply a correction. Probably the easiest thing to observe is the perturbed electric field, which would appear as an error in module voltage as a function of time during bunch passage. The negative of this error could be applied to the bunch a hundred meters or less down stream. To see how this would work, replace eqn. (2') by:

$$\frac{\partial}{\partial z}\frac{\delta v}{v_0} = \mathcal{E}(z) - \mathcal{E}(z-\ell) \sim \ell \frac{\partial \mathcal{E}}{\partial z} \qquad (2'')$$

where ℓ is the feed-forward distance.

A simple dispersion analysis of (1'), (2") and (3') leads to a damping factor, $\exp\left[-\frac{\omega^7\tau^7}{1+\omega^2\tau^2}K^2\ell z\right]$, which is indicative but misleading in that the apparent advantage of making ℓ large is due to the Taylor expansion approximation in (2"). Figure 3 shows the results of a simulation in which the perturbation grows from noise and in the right hand plot is fed forward at a distance of 100 meters. Much remains to be studied about this scheme, but it looks promising.

IV. CONCLUSION

This instability can be overcome by manipulating R and C of the modules, but at the price of reduced efficiency and increased cost. We shall continue to look for a compromise by involving a feed-forward system and a tolerable momentum spread. We have to rely heavily on theoretical analysis for now since there is no possibility of realistic experimental study without an accelerator capable of handling some hundreds of amperes. A group at the University of Maryland is planning a model experiment using low-energy electrons [2], from which we hope to gain considerable information.

V. REFERENCES

[1] For more details, see E.P. Lee and L. Smith, "Asymptotic Analysis of the Longitudinal Instability of a Heavy Ion Induction Linac," Proc. 1990 Linac Conf. p. 716-718, September 1990. See also E.P. Lee and L. Smith, "Analysis of Resonant Longitudinal Instability in a Heavy Ion Induction Linac," paper LRA62, this conference.

[2] J.G. Wang et al., "Resistive Wall Instability Experiment at the University of Maryland," paper LTP17, this conference.

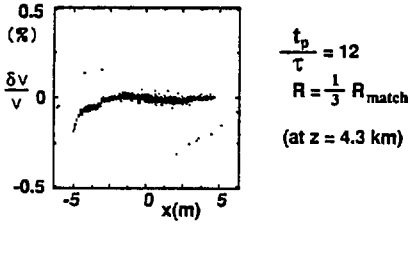

Fig. 3. Phase space plots with and without feed-forward correction. External impedance is assumed to be represented by parallel R and C.

Analysis of Resonant Longitudinal Instability in a Heavy Ion Induction Linac*

Edward P. Lee and L. Smith
Lawrence Berkeley Laboratory
University of California, Berkeley, California 94720

SUMMARY

A high current beam of subrelativistic ions accelerated in an induction linac is predicted (in some circumstances) to exhibit unstable growth of current fluctuations at high frequencies ($\nu \sim 100$ MHz). The instability is driven by the interaction between the beam and accelerator modules at frequencies close to a cavity resonance. The extent of unstable growth depends on features of the coupling impedance, beam parameters, and total pulse and accelerator lengths. Transient and asymptotic analysis is presented.

Induction Linac Model

We treat a cluster of beams drifting at velocity v, with line charge density λ and current $I = \lambda v$. It is assumed here that all the beamlets ($N \sim 16$) effectively act in concert so that λ and I are the total values and v is the common velocity. The continuity equation, using laboratory frame variables (z,t) is:

$$\frac{\partial \lambda}{\partial t} + \frac{\partial I}{\partial z} = 0 \ . \tag{1}$$

The beam cluster is treated as a cold, 1-d, non-relativistic fluid. An externally imposed field E^{ex} and a smoothed longitudinal field E, induced by interaction of I with the acceleration modules, acts on v:

$$\frac{\partial v}{\partial t} + v \frac{\partial v}{\partial z} = \frac{q}{m}\left(E + E^{ex}\right) \ . \tag{2}$$

Neglected in this model are velocity spread and a direct space-charge force proportional to $\partial\lambda/\partial z$. These are significant stabilizing features at the high frequencies treated here, so the calculation may be considered pessimistic. The purpose of the present work is to delineate the phenomena of the longitudinal instability occuring in heavy ion induction linacs, and to guide future study. The analysis is similar to that given by V. K. Neil[1] for relativistic electron beams.

The equilibrium beam drifts at constant velocity v_o, so the total equilibrium field $(E_o + E_o^{ex})$ vanishes. Equilibrium current I_o and line charge density λ_o are, in general, functions of the retarded time $\tau = t - z/v_o$. However, they are taken to be constant for the duration of the pulse $(0 < \tau < \tau_p)$.

*Work was supported by the Director, Office of Energy Research, Office of Basic Energy Sciences, Advanced Energy Projects Division, U.S. Dept. of Energy under Contract No. DE-AC03-76SF00098.

Let E^{ex} have a small additional component which acts at $z = o$ and therefore perturbs the beam: $E^{ex} = E_o^{ex} + V(t)\delta(z)$. From eqns. (1) and (2) the resulting perturbed beam variables satisfy

$$\frac{\partial \lambda_1}{\partial t} + \frac{\partial I_1}{\partial z} = 0 \ , \tag{3}$$

$$\frac{\partial v_1}{\partial t} + v_o \frac{\partial v_1}{\partial z} = \frac{q}{m}\left(E_1 + V\delta(z)\right) \ , \tag{4}$$

$$I_1 = \lambda_o v_1 + v_o \lambda_1 \ .$$

Module Response

The beam-generated field E_1 is induced by by the passage of the return current $(-I_1)$ through the module impedance Z. If we assume the driven form $I_1 \sim \exp(-i\omega t)$, with induced field $E_1(\omega)$, then impedance is

$$Z(\omega) = -E_1(\omega)/I_1 \ . \tag{5}$$

Specifically, we treat an isolated module resonance characterized by a parallel L-R-C equivalent circuit:

$$C\frac{\partial^2 E_1}{\partial t^2} + \frac{1}{R}\frac{\partial E_1}{\partial t} + \frac{E_1}{L} = -\frac{\partial I_1}{\partial t} \ . \tag{6}$$

The circuit parameters are related to measured resonance features; let R be the real impedance peak (units of Ω/m in the smoothed field model), occuring at angular frequency ω_o. and resonance width is $\Delta\omega = \omega_o/Q$ at 71% of maximum |Z|. Then we have

$$C = Q/\omega_o R \ \text{(F-m)}, \quad LC = \omega_o^{-2} \ . \tag{7}$$

The impedance formula for general (complex) ω is

$$Z = \left(\frac{1}{R} - i\omega C - \frac{1}{i\omega L}\right)^{-1} = \frac{R}{1 - iQ\left(\frac{\omega}{\omega_b} - \frac{\omega_b}{\omega}\right)} \ . \tag{8}$$

Typical resonance parameters of interest for the Heavy Ion Fusion application are $\nu_o = \omega_o/2\pi = 30$–$300$ MHz, $Q = 10$-100, and $R = 100$-$1000\ \Omega$/m.

Beam Frame Equations

It convenient to use the retarded time variable $\tau = t - z/v_o$ and z instead of the laboratory frames variables t and z. Then eqns. (3) and (4) become

$$\frac{\partial I_1}{\partial z} = \frac{\partial}{\partial \tau}\frac{\lambda_o v_1}{v_o}, \tag{9}$$

$$\frac{\partial v_1}{\partial z} = \frac{q e}{m v_o}\left[E_1 + \delta(z)\, V(\tau)\right]. \tag{10}$$

We eliminate v_1 to obtain

$$\frac{\partial^2 I_1}{\partial z^2} = \frac{\partial}{\partial \tau}\, K^2 C\left[E_1 + \delta(z)\, V(\tau)\right], \tag{11}$$

where

$$K^2 = \frac{q e \lambda_o}{m v_o^2 C}. \tag{12}$$

Equation (6) becomes

$$\left(\frac{\partial^2}{\partial \tau^2} + \frac{\omega_o}{Q}\frac{\partial}{\partial \tau} + \omega_o^2\right) E_1 = -\frac{1}{C}\frac{\partial I_1}{\partial \tau}. \tag{13}$$

The natural scale frequencies for z and τ are K and ω_o. Generally the scale magnitude $\omega_o \tau \sim 300$ is much larger than $Kz \sim 10$. Eqns.(11) and (13) describe strongly coupled oscillations in both τ and z, which exhibit growth in both variables. We expect large growth in τ will be produced by an external perturbation $V(\tau)$ which contains any appreciable content near the resonant frequency ω_o. In eqns. (11)-(13), K may be a function of τ, however a numerical treatment would then be required. Henceforth K is taken to be constant.

The perturbation $V(\tau)$ is assumed to turn on within the beam pulse at some $\tau = \tau_o > o$. The structure of the coupled equations ensures that perturbed quanatities may be consistently assumed to vanish outside the zones $\tau \geq \tau_o$, $z \geq o$.

General Solution by Laplace Transformation

Taking E_1 and I_1 to vanish for $(\tau < \tau_o, z < o)$, we find from eqn. (11) the initial conditions at $z = o+$:

$$I_1(o+) = o, \quad \frac{\partial I_1}{\partial z}(o+) = \frac{q e \lambda_o}{m v_o^2}\frac{\partial V}{\partial \tau}. \tag{14}$$

Performing the Laplace transformation

$$\left(\hat{I}_1, \hat{E}_1\right) = \int_o^\infty d\tau\, e^{i\omega\tau}\left(I_1, E_1\right), \tag{15}$$

we get

$$\frac{\partial^2 \hat{I}_1}{\partial z^2} = -K^2 C i\omega \hat{E}_1 = (\omega\Gamma K)^2 \hat{I}_1, \tag{16}$$

with

$$\Gamma = \left(\omega_o^2 - \omega^2 - i\omega\omega_o/Q\right)^{1/2}.$$

The solution $\hat{I}_1$ satisfying the initial conditions (14) is

$$\hat{I}_1 = \left(\frac{q e \lambda_o}{m v_o^2}\right)\left(-i\omega \hat{V}\right)\frac{\sinh(\omega\Gamma K z)}{(\omega\Gamma K)}. \tag{17}$$

The inverse transformation is

$$I_1 = \frac{1}{2\pi}\int_{-\infty}^{+\infty} d\omega\, e^{-i\omega\tau}\hat{I}_1. \tag{18}$$

with all singularities below the real ω axis.

Asymptotic Growth Formulas

The general character of resonant growth can be determined by the saddle point method. The form of I_1, given by eqn (18) is

$$I_1 \sim \int_{-\infty}^{+\infty} d\omega\, f(\omega)\exp(g), \tag{19}$$

with

$$g = -i\omega\tau \pm \omega\Gamma K z. \tag{20}$$

Intrinisic singularities are located at the complex resonance values (poles of Γ^2),

$$\omega = \pm\bar{\omega} - i\omega_o/2Q, \tag{21}$$

where

$$\bar{\omega} = \omega_o\sqrt{1 - 1/(2Q)^2}.$$

Saddle points are located at the six roots of the equation

$$0 = \frac{\partial g}{\partial \omega} = -i\tau \pm K z \Gamma\left[1 + \Gamma^2\omega\left(\omega + i\omega_o/2Q\right)\right]. \tag{22}$$

The integration contour in eqn (19) can be deformed to pass through the saddle points, and the dominant contributions to I_1 are produced at these locatons for sufficiently large z and τ. To simplify the saddle calculaton let

$$u = \omega/\bar{\omega} + i\varepsilon, \quad \varepsilon = \omega_o/2\bar{\omega}_o Q \tag{23}$$

assumed small compared with unity. Then eqns. (20) and (21) become (at the saddles)

$$g = -i\bar{\omega}\tau\frac{u(u - i\varepsilon)^2}{(1 - i\varepsilon u)}, \tag{24}$$

$$(u^2 - 1)^3 = \left(\frac{Kz}{\bar{\omega}\tau}\right)^2(1 - i\varepsilon u)^2. \tag{25}$$

For mode growth associated with the module resonance we expect $u \approx \pm 1$, which requires $\bar{\omega}\tau >> Kz$, Eqn. (25) gives

$$u^2 = 1 + r\left(\frac{Kz}{\bar{\omega}\tau}\right)^{2/3}(1 - i\varepsilon u)^{2/3}, \tag{26}$$

where r is any cube root of unity. The small quantity $\varepsilon = (2Q)^{-1}$ is a fixed constant. However we shall find that at peak growth for fixed z, $(Kz/\bar{\omega}\tau)$ is of order $\varepsilon^{3/2}$. To solve eqn (26) by an expansion in the small parameters we formally define

$$\beta \equiv \frac{(Kz/\bar{\omega}\tau)^{2/3}}{\varepsilon}, \tag{27}$$

and regard β as of order unity. The resulting expressions for u and g are, assuming $u = +1$,

$$u = 1 + \frac{\varepsilon\beta r}{2} - \varepsilon^2\left(\frac{\beta^2 r^2}{8} + \frac{i\beta r}{3}\right) + \dots, \tag{28}$$

$$g = -i\bar{\omega}\tau\left[1 + \varepsilon\left(\frac{3\beta r}{2} - i\right) + \varepsilon^2\left(\frac{3\beta^2 r^2}{8} - i\beta r\right) + \dots\right]. \tag{29}$$

For unstable growth the relevant cube root of unity is $r = (\sqrt{3}\, i-1)/2$. We get, keeping only terms through order ε:

$$g_r = \frac{3\sqrt{3}}{4}(\bar{\omega}\tau)^{1/3}(Kz)^{2/3} - \frac{\omega_b\tau}{2Q}, \tag{30}$$

$$g_i = -\bar{\omega}\tau + \frac{3}{4}(\bar{\omega}\tau)^{1/3}(Kz)^{2/3}. \tag{31}$$

At specified z the maximum value of g_r is readily found from eqn (30):

$$0 = \frac{\partial g_r}{\partial\tau} = \bar{\omega}\left[\frac{\sqrt{3}}{4}\left(\frac{Kz}{\bar{\omega}\tau}\right)^{2/3} - \varepsilon\right]. \tag{32}$$

At this point $\beta = 4/\sqrt{3}$, which is of order unity, as assumed. The maximum growth factor is

$$(g_r)_{max} = \left(\frac{\sqrt{3}}{2}\right)^{3/2}\left(\frac{\bar{\omega}Q}{\omega_b}\right)^{1/2} Kz. \tag{33}$$

Application to Heavy Ion Fusion

The maximum growth is calculated here at a medium energy position in a fusion driver, with ion parameters (T = 1000 MeV, m = 200 amu, q = 1), and the typical pulse parameters ($I_0 = 10^3$ A, $\tau_p = 500$ ns.) For the module response we take $\bar{\omega} \equiv \omega_0 = 2\pi\times10^8\ s^{-1}$, Q = 30, R = 300 Ω/m. Then we have

$$v_o = .104c,\ \lambda_o = 32.2\ \mu C/m,$$

$$C = 10^{-9}/2\pi\ F\text{-}m,\ K = .0100\ m^{-1}.$$

At the pulse end $\bar{\omega}\tau_p = 314$ and the maximum growth point is

$$z = \frac{\bar{\omega}\tau_p}{K}\left(\frac{2}{\sqrt{3}\,Q}\right)^{3/2} = \frac{2.36}{K} = 236\ m,$$

$$(g_r)_{max} = \left(\sqrt{3}/2\right)^{3/2} Q^{1/2}\, Kz = \omega_b\tau_p/Q = 10.5.$$

This calculated total growth [exp(10.5) = 36300] is large enough to be of concern, even though the initial disturbance $V(\tau)$ may be very small in the unstable band. A small rms velocity spread $\left(\Delta v/v_o \approx v_o(g_r)_{max}/\omega_b z_{max} \approx .0022\right)$ would be sufficient to eliminate growth, but would constrain the focal spot radius achievable in a fusion reactor.

Dispersion Relation

A Laplace transformation in both τ and z on eqns (11)-(13) yield

$$I_1 \sim \int d\omega \int d\Omega \frac{F(\omega)}{D} e^{-i(\omega\tau+\Omega z)}, \tag{34}$$

where the dispersion relation is

$$D(\omega,\Omega) = -K^2\omega^2 + i\omega\Omega^2/CZ(\omega) \tag{35}$$

$$= \left(\omega^2 - \omega_0^2 + i\omega\omega_b/Q\right)\left(\Omega^2 - K^2\right) - K^2\left(\omega_0^2 - i\omega\omega_b/Q\right). \tag{36}$$

The latter form of D clearly indicates that a pair of strongly coupled resonances are present, and appear symmetrically when $Q = \infty$. A growth formula, valid for near resonance $\Omega^2 \approx K^2$, may therefore be obtained from eqn. (30) by interchanging $\omega_o\tau$ with Kz. For $Kz >> \omega_o\tau$ we have

$$g_r = \left(3\sqrt{3}/4\right)(\omega_b\tau)^{2/3}(Kz)^{1/3}, \tag{37}$$

$$g_i = -Kz + (3/4)(\omega_b\tau)^{2/3}(Kz)^{1/3}. \tag{38}$$

The roots of the dispersion equation $D(\omega,\Omega) = 0$ can be used to find the growth in z for given real ω; we find for the imaginary part of Ω

$$\Omega_i = \left[\frac{K^2C\omega}{2}\left(|Z| - Z_i\right)\right]^{1/2}, \tag{39}$$

with

$$Z = Z_r + iZ_i = \frac{R\left[1 + iQ\left(\frac{\omega}{\omega_b} - \frac{\omega_b}{\omega}\right)\right]}{1 + Q^2\left(\frac{\omega}{\omega_b} - \frac{\omega_b}{\omega}\right)^2}.$$

The maximum growth formula .. (33) may be recovered from eqn. (39) for large Q by maximizing Ω_i with respect to driving frequency ω.

Reference

[1] V. K. Neil, Interaction of the ATA Beam with the TM030 Mode of the Accelerating Cells, LLNL report UCID-20456, 1985.

HIFAR STAFF ROSTER

Roger Bangerter
Warren Chupp
Robert D. Edwards
Shmuel Eylon
Andris Faltens
Thomas J. Fessenden
Craig Fong
Terence Garvey
William B. Ghiorso
Wayne Greenway
Ralph Hipple
Cai Houston
Rudin Johnson
Huan-Ju Lee
Carl Lionberger
Sam Mukherjee
Harry Meyer
Joseph Perez
Chester D. Pike
John Pruyn
Thomas Purtell
James Rice, Jr.
Henry L. Rutkowski
Gerald L. Stoker
Bill Tiffany
David Vanecek
Gerald West

Lloyd Smith
Elon Close
William Fawley
Kyoung Hahn
Enrique Henestroza
David L. Judd
L. Jackson Laslett
Edward P. Lee

Clerical Staff

Joy Kono
Diana Morris
Alline Tidwell
Olivia Wong

LLNL

Louis L. Reginato

SLAC

William B. Herrmannsfeldt

Students

Eric Agol
Miguel Nathwani
Dan Keeney

PUBLICATIONS AND INTERNAL NOTES

HIFAN-478
LBL-29743
HIFAR Group

HIFAR Group
Heavy Ion Fusion Accelerator Research (HIFAR), Year-End Report. April 1, 1990 - September 30, 1990.

HIFAN-479
LBL-29827
Hahn

Kyoung D. Hahn
"Longitudinal Instability in heavy ion fusion driver and feedback stabilization," to be presented at the IAEA Technical Commmittee Meeting on Drivers for Inertial Confinement Fusion, Osaka, Japan, April 15-19, 1991.

HIFAN-480
LBL-30102
Bangerter

Roger O. Bangerter
"Heavy Ion Driver Development in the U.S."
Invited paper for the IAEA Technical Commmittee Meeting on Drivers for Inertial Confinement Fusion, Osaka, Japan,
April 15-19, 1991.

HIFAN-481
LBL-30140a
Fessenden

Thomas J. Fessenden
"Summary of the International Symposium on Heavy Ion Inertial Fusion." Abstract submitted to the International Topical Conference on Research Trends in Inertial Confinement Fusion,
February 4-6, 1991.

HIFAN-482
LBL-30029a
Fessenden

Thomas J. Fessenden
"Emittance Variations in Current-Amplifying Ion Induction Linacs,"
Invited Abstract submitted to 1991 IEEE Particle Accelerator Conference, Accelerator Science and Technology (Annual Meeting of the APS Division of Beam Physics), May 6-9, 1991, Sheraton Palace Hotel, San Francisco, CA.

HIFAN-483
LBL-30030a
Berz

M. Berz, W. Fawley and K. Hahn
"High Order Calculation of the Multipole Content of Three Dimensional Electrostatic Geometries,"
Abstract submitted to 1991 IEEE Particle Accelerator Conference, Accelerator Science and Technology (Annual Meeting of the APS Division of Beam Physics), May 6-9, 1991, Sheraton Palace Hotel, San Francisco, CA.

HIFAN-484
LBL-30058a
Faltens

Andris Faltens
"Induction Accelerator Test Module for HIF,"
Abstract submitted to 1991 IEEE Particle Accelerator Conference, Accelerator Science and Technology (Annual Meeting of the APS Division of Beam Physics), May 6-9, 1991, Sheraton Palace Hotel, San Francisco, CA.

HIFAN-485
LBL-30069a
Lee

Edward P. Lee and Lloyd Smith
"Analysis of Resonant Longitudinal Instability in a Heavy Ion Induction Linac,"
Abstract submitted to 1991 IEEE Particle Accelerator Conference, Accelerator Science and Technology (Annual Meeting of the APS Division of Beam Physics), May 6-9, 1991, Sheraton Palace Hotel, San Francisco, CA.

HIFAN-486
LBL-30070a
Eylon

S. Eylon, E. Henestroza, T. Garvey, R. Johnson and W. Chupp
"Low-Emittance Uniform-Density Cs^+ Sources for Heavy Ion Fusion Accelerators Studies,"
Abstract submitted to 1991 IEEE Particle Accelerator Conference, Accelerator Science and Technology (Annual Meeting of the APS Division of Beam Physics), May 6-9, 1991, Sheraton Palace Hotel, San Francisco, CA.

HIFAN-487
LBL-30071a
Rutkowski

H.L. Rutkowski, A. Faltens, C. Pike, D. Brodzik, R.M. Johnson and D. Vanecek
"An Induction Linac Injector for Scaled Experiments,"
Abstract submitted to 1991 IEEE Particle Accelerator Conference, Accelerator Science and Technology (Annual Meeting of the APS Division of Beam Physics), May 6-9, 1991, Sheraton Palace Hotel, San Francisco, CA.

HIFAN-488
LBL-30206a
Smith

Lloyd Smith
"Longitudinal Instability in HIF Beams,"
Invited Abstract submitted to 1991 IEEE Particle Accelerator Conference, Accelerator Science and Technology (Annual Meeting of the APS Division of Beam Physics), May 6-9, 1991, Sheraton Palace Hotel, San Francisco, CA.

HIFAN-489
LBL-30205a
Eylon

S. Eylon, A. Faltens, W. Fawley, T. Garvey, K. Hahn, E. Henestroza and L. Smith
"Drift compression experiments on MBE-4 and related emittance growth phenomena," Abstract submitted to 1991 IEEE Particle Accelerator Conference, Accelerator Science and Technology (Annual Meeting of the APS Division of Beam Physics), May 6-9, 1991, Sheraton Palace Hotel, San Francisco, CA.

HIFAN-490
LBL-30208a
Garvey

T. Garvey, S. Eylon, T.J. Fessenden, K. Hahn, and E. Henestroza
"Transverse Emittance Studies of an Induction Accelerator of Heavy Ions," Abstract submitted to 1991 IEEE Particle Accelerator Conference, Accelerator Science and Technology (Annual Meeting of the APS Division of Beam Physics), May 6-9, 1991, Sheraton Palace Hotel, San Francisco, CA.

HIFAN-491
Bangerter

Roger Bangerter, "Heavy Ion Fusion-Progress and Prospects," invited paper presented at the International Symposium on Heavy Ion Inertial Fusion, December 3-6, 1990, Monterey, CA, LBL-30334a.

HIFAN-492
Lee

Edward P. Lee, "Longitudinal Instability of Induction Linac Drivers," paper presented at the International Symposium on Heavy Ion Inertial Fusion, December 3-6, 1990, Monterey, CA, LBL-30335a.

HIFAN-493
Garvey

T. Garvey, S. Eylon, T.J. Fessenden and E. Henestroza, "Beam Acceleration Experiments on a Heavy Ion Linear Induction Accelerator (MBE-4)," paper presented at the International Symposium on Heavy Ion Inertial Fusion, December 3-6, 1990, Monterey, CA, LBL-30336a.

HIFAN-494
Rutkowski

Henry L. Rutkowski, A. Faltens, C. Pike, D. Brodzik, D. Vanecek, "The Berkeley Injector," paper presented at the International Symposium on Heavy Ion Inertial Fusion, December 3-6, 1990, Monterey, CA, LBL-30337a.

HIFAN-495
Close

E. Close, C. Fong, E. Lee, "HILDA: Heavy Ion Linac Analysis Code," paper presented at the International Symposium on Heavy Ion Inertial Fusion, December 3-6, 1990, Monterey, CA, LBL-30338a.

HIFAN-496
Hahn

K. Hahn and L. Smith, "Time Domain Analysis of 1-D Longitudinal Beam Dynamics in an Induction Linac," paper presented at the International Symposium on Heavy Ion Inertial Fusion, December 3-6, 1990, Monterey, CA, LBL-30339a.

HIFAN-497
LBL-30340
Faltens

A. Faltens, S. Mukherjee, V. Brady, "The Development of Compact Magnetic Quadrupole for Heavy Ion Accelerators," paper presented at the International Symposium on Heavy Ion Inertial Fusion, December 3-6, 1990, Monterey, CA, LBL-30340a.

HIFAN-498
Eylon

S. Eylon, E.R. Colby, T.J. Fessenden, T. Garvey, K. Hahn and E. Henestroza, "Emittance Variations of Very Cold Ion Beams During Transport Through MBE-4," paper presented at the International Symposium on Heavy Ion Inertial Fusion, December 3-6, 1990, Monterey, CA, LBL-30341a.

HIFAN-499
Berz
(02/12/91)

Martin Berz, William M. Fawley and Kyoung Hahn, "High order calculation of the multipole content of three dimensional electrostatic geometries," submitted to Nuclear Instruments and Methods in Physics Research, Institute of Physics, February 1991 (LBL-30322)

HIFAN-500
HIFAR GROUP

DoE HIFAR Review, March 26, 1991, Bldg. 71 Conference Room

HIFAN-501

HIFAR Program Technical Briefing, DoE, March 14, 1991, Bangerter, Lee, Washington, DC.

Fessenden

HIFAN-502
Fessenden
(03/13/91)

Report on the International Symposium held at Monterey, California, December 3-6, 1990, "Heavy Ion Inertial Fusion," Thomas J. Fessenden, LBL; Alex Friedman, LLNL.

HIFAN-503
Fessenden
3/18/91

"MBE-4 Experiments with bright Cesium$^+$ beams"
Abstract

HIFAN-504
Bangerter
04/12/91

Discussion of Heavy Ion Fusion Accelerator Research, April 12, 1991, with Dr. James F. Decker, Acting Director, Office of Energy Research and Dr. N. Anne Davies, Acting Associate Director, Office of Fusion Energy.

HIFAN-505
Bisognano
4/30/90

J. Bisognano, K. Bane, R. Briggs, A. Faltens, A. Friedman, G. Lambertson, B. Langdon, E. Lee, J. Leiss, R. Shafer, L. Smith, P. Sprangle, and P. Wilson,
"Report on Heavy Ion Induction Linac Workshop", April 30-May 1, 1990.

HIFAR NOTES (Internal and Informal)

HIFAR Note 285 Garvey	Transverse Emittance Measurements on MBE-4, Terry Garvey, E. Henestroza and S. Eylon, 01/01/91
HIFAR Note 286 Crandall	Final-Focus Design Assumptions for HIF Scaling Experiment, Ken Crandall, AccSys, January 24, 1991
HIFAR Note 287 Judd	Some Simple Features of Beam Dynamics Relative to a "Twisted Circular" Orbit, David Judd, August 1990.
HIFAR Note 288 Lionberger	Status of HIF Experimental Software, Carl Lionberger, February 6, 1991
HIFAR Note 289 Fessenden/Eylon	Termination of MBE-4 Experiments, Tom Fessenden & Shmuel Eylon, February 8, 1991
HIFAR Note 290 HIFAR Staff	U.S. Department of Energy Field Task Proposal/Agreement April 1, 1991
HIFAR Note 291 J. West	MBE-4 Ion Source Line Voltage Stabilizer
HIFAR Note 292 D. Brodzik	One, Two MV Marx - Load and Rep Rate Considerations, March 20, 1991.
HIFAR Note 293 D. Brodzik	Inductively Graded Marx - Protective Devices, March 25, 1991.
HIFAR Note 294 D. Brodzik	Current Valve Pulser, March 25, 1991.
HIFAR Note 295 Carl Lionberger	Recent Modifications to Show.pas, March 28, 1991.
HIFAR Note-296 J. Stoker	SBTS Marx Column Voltage Gradient Divider April 8, 1991
HIFAR Note-297 E. Henestroza 05/14/91	Longitudinal motion of a beam crossing an electrostatic MBE4 quadrupole doublet, E Henestroza, May 14, 1991.
HIFAR-298 E. Henestroza 05/15/91	Ion source simulations for the Final Focus Scaling Experiment, E. Henestroza, May 15, 1991.

HIFAR-299
D. Vanecek

Building 58 Slab Motion
5/20/91

HIFAR Note-300
V. Brady

2D Field Calculations for ILSE Prototype Quad
May 17, 1991

HIFAR Note-301
E. Lee

Memo To: ILSE Team Subject: Transport Limits in ILSE
May 23, 1991